

# A consistent variational approach for coupling 3D–1D models

P.J. Blanco <sup>a,\*</sup>, R.A. Feijóo <sup>a</sup> and S.A. Urquiza <sup>b</sup>

<sup>a</sup>*LNCC, Laboratório Nacional de Computação Científica, Av. Getúlio Vargas 333, Quitandinha, 25651-075, Petrópolis, RJ, Brazil, e-mail: pjblanco@lncc.br, feij@lncc.br*

<sup>b</sup>*Laboratorio de Bioingeniería, Universidad Nacional de Mar del Plata, Av. J.B. Justo 4302, 7600 Mar del Plata, Argentina, e-mail: santiagourquiza@fi.mdp.edu.ar*

---

## Abstract

In this work, we propose an extended variational formulation in order to handle the problem of the flow of an incompressible fluid in compliant vessels with discontinuous fields. This approach makes possible to tackle in a consistent variational manner problems like the coupling between models of different dimensionality. This approach is used in the context of modelling blood flow in large vessels. A computational implementation of the proposed formulation is also shown and discussed by presenting examples of practical applications.

*Key words:* Variational formulation, discontinuous fields, coupling conditions, multidimensional models, hemodynamics.

---

## 1 Introduction

Computational modelling provides a powerful tool to study and correlate the onset and progress of some cardiovascular diseases with the local patterns of the blood flow [6,11,21,32]. Accordingly, the detailed modelling of fluid mechanics processes on some specific arterial districts has become increasingly important to understand the local hemodynamic phenomena [23,27].

Modelling the fluid mechanics aspects of blood flow involves several challenging issues that must be accounted for in order to achieve ever-increasing levels

---

\* Corresponding author.

*Email address:* pjblanco@lncc.br (P.J. Blanco).

of realism in computational simulations. Among others, one of the most relevant aspects of the problem is the fluid–structure interaction derived from the coupling between the compliant properties of the vessel walls and the blood flow. This feature defines the propagatory nature of the pulse wave which, in turn, poses the problem of setting appropriate boundary conditions when a particular district is artificially isolated from the rest of the network. It is possible to mention at least three ways of tackling this subject: the classical one is based on obtaining boundary conditions by estimations or measurements (see for instance [25,26]). The second one, presented recently in [35], is based on computing what was called a Dirichlet–to–Neumann mapping that takes into account the phenomena occurring downstream the 3D region through the computation of the downstream vascular impedance. However, this method is actually derived only for outflow boundary conditions and also under time–periodic assumptions, which may result too restrictive to accommodate the complex situations encountered in practice. Finally, the third possibility is based on the use of coupled 3D–1D models where some zones are modelled at a high level of detail (3D domain) while the remaining part of the system is simplified to a 1D formulation or even to a 0D lumped model. In this way, it is possible to achieve in a natural manner the systemic response of the whole arterial tree [9,10,33]. While the second approach is by far more suitable than the classical one, is the later the more appropriate in order to consider all the complex interactions that occur within the whole system operating as a fully integrated functional ensemble. This assertion must be understood regarding the capability of automatically adapting boundary conditions to what happens beyond the limits of the 3D domain, either in time–varying conditions or during parameter adjustment in the context of sensitivity analysis.

Several authors [9,33] have treated the problem of coupling full 3D models based on the Navier Stokes equations in compliant domains with reduced 1D models by making a priori assumptions directly incorporated into the partial differential equation problem. This is done by prescribing the continuity of some of the involved quantities (for instance flow rate and mean pressure) at the coupling interfaces. Nevertheless, it must be noted that discontinuities may emerge from the use of incompatible models at both sides of a given coupling interface because of differences in the underlying kinematics, as well as from the use of different levels of approximation for each part of the original domain. For instance, in ref. [33], the continuity of the pressure (actually the normal traction) between 3D and 1D models is stated in a weak sense. This, in turn, implies, in a point–wise sense, the existence of a possible jump in the pressure field when dealing with the corresponding discrete problem. Moreover, when using elastic models for the arterial wall the area is uniquely determined by the value of the internal pressure. As a consequence, the area of the vessel at both sides of the coupling interfaces may differ from each other. This issue was treated in [33] by relaxing the continuity of the cross sectional area, in contrast to that suggested in [9] where this condition was stated as one of the coupling

requirements. Consequently, the former alternative conducts to efficient fully coupled schemes where numerical instabilities are practically avoided in contrast to that reported by Formaggia et al., [9]. Despite that, several other sources of discontinuities may be noticed from the non-matching kinematics over the coupling interfaces. For example, the abrupt change on the shape of the velocity profile across an artificial internal boundary carries out relative jumps on the linear momentum and wall shear stress. Observe that such a change in the velocity profile can be interpreted as being consequence of a selection of somehow incompatible kinematical reduction hypothesis over the 1D portion of the model. Conversely, in ref. [10,13] the coupling of multidimensional models is understood as a problem with a priori defective boundary conditions on the 3D model due to the mismatch between the information available at both sides of the interfaces. In fact, in those works the theory for 3D models with boundary conditions based upon mean quantities is developed. Within this approach the problem is interpreted as ill-posed since one has full 3D fields at one side of the interface and only mean quantities at the other side. Consequently, some supplementary assumptions are introduced in order to “close” the problem.

Alternatively, the present work aims at tackling this situation from a different perspective. Observe that a  $ND$  ( $N = 0, 1, 2$ ) simplified model can be viewed as a reduction of a complete 3D model by means of kinematical restrictions introduced on a part of a given domain. Performing such kinematical assumptions allows us to reduce the full problem over that part of the domain to a 2D, a 1D or even a 0D lumped problem. By looking at the whole domain again we realize that, due to the dissimilarity between the underlying kinematics, we generated discontinuities in the involved fields. Therefore, the original variational formulation, valid for fields that are continuous in the sense of the trace of the functions over such a coupling interface, makes no sense in this new situation. For this reason it is necessary to reformulate the problem, rewriting the variational principle in order to accommodate those discontinuities. Hence, the main goal of the present work is to formulate an extended variational principle for problems where fields can become discontinuous at some artificial internal boundary, that will be regarded as the coupling interface. Moreover, we recast this problem within a unified variational statement from which the coupling conditions are naturally derived. The conception of such a consistent unified variational formulation of the coupled problem is very desirable when performing, for instance, stability and error analysis on the corresponding numerical schemes.

Although the application of these ideas to hemodynamic modelling is of our main concern, this issue is inherent to a great variety of problems, and other examples can easily be devised. For instance, the fluid-structure interaction problem may involve different interpolations for the fluid and the solid domain, as well as joining 3D solid models with shell models or even beam components

may lead to discontinuous fields.

This work is organized as follows, in Section 2 a simple example is conducted so as to outline the ideas behind this approach, formulating the coupling between models of different dimensionality for the heat transfer problem. In Section 3 we address a classical statement for the problem of the flow of an incompressible fluid in a compliant vessel, whilst in Section 4 this problem is extended within the theoretical context of discontinuous fields. In Section 5 an approximation of the problem presented in Section 4 is performed and a discrete counterpart is given. Finally, in Section 6 several numerical experiments are presented illustrating the capabilities of this approach in cardiovascular modelling. In addition, situations where spurious reflections arise are identified.

## 2 Extended variational formulation for the heat transfer problem

In this section we present a simple example where the main idea of extending a variational statement is introduced. Let  $\Omega \subset \mathbb{R}^{n_d}$  ( $n_d = 2, 3$ ) with boundary  $\Gamma$  and consider the variational formulation for the heat transfer problem: *find*  $\theta \in \mathcal{X}$  *such that*

$$\int_{\Omega} k \nabla \theta \cdot \nabla \eta \, d\mathbf{x} = \int_{\Omega} f \eta \, d\mathbf{x} \quad \forall \eta \in \mathcal{Y}, \quad (1)$$

where  $k$  is the conductivity coefficient assumed to be constant for the sake of simplicity and  $f$  is a volume source. Regularity and essential boundary conditions are accounted by the set  $\mathcal{X}$ , while space  $\mathcal{Y}$  accounts for admissible variations of functions in  $\mathcal{X}$ . For this example it is well-known that we have  $\mathcal{X} = \{\theta \in H^1(\Omega); \theta = \bar{\theta} \text{ on } \Gamma_D\}$ , being  $\Gamma_D$  the Dirichlet boundary. Without loss of generality we consider that  $\Gamma_D = \Gamma$ .

Let  $\Gamma_c$  be an artificial internal boundary that allows us to make a partition of domain  $\Omega$ , according to Figure 1 (here a 2D domain for simplicity), into subdomains  $\Omega_1$  and  $\Omega_2$  with boundaries  $\Gamma_1$  and  $\Gamma_2$  respectively. Thus we have  $\Omega = \Omega_1 \cup \Omega_2 \cup \Gamma_c$ ,  $\Gamma_c = \Gamma_1 \cap \Gamma_2$  and  $\Gamma = (\Gamma_1 \cup \Gamma_2) \setminus \Gamma_c$ .

As a consequence of the regularity of functions in  $\mathcal{X}$  we have that the traces of  $\theta_1$  and  $\theta_2$  coincide over boundary  $\Gamma_c$ , and we must also consider that  $\theta = \bar{\theta}$  on  $\Gamma_D$ . Hence, the Euler equations and the Weierstrass–Erdmann corner conditions associated to the variational problem (1), regarding the splitting of

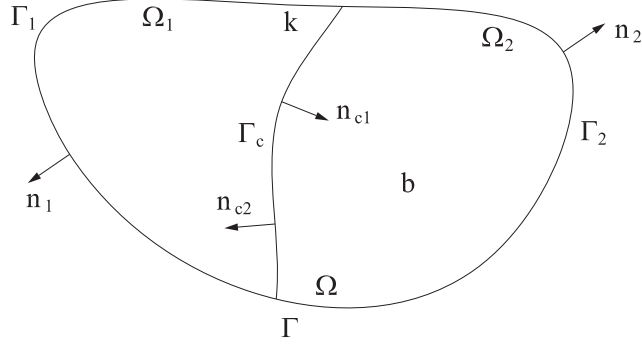


Fig. 1. Split of domain  $\Omega$ .

the domain  $\Omega$ , are given by

$$\begin{cases} -k\Delta\theta_1 = f & \text{in } \Omega_1, \\ -k\Delta\theta_2 = f & \text{in } \Omega_2, \\ k\nabla\theta_1 \cdot \mathbf{n}_{c1} = k\nabla\theta_2 \cdot \mathbf{n}_{c1} & \text{on } \Gamma_c, \end{cases} \quad (2)$$

where  $\mathbf{n}_{c1}$  is the unit normal vector of boundary  $\Gamma_c$  (from domain  $\Omega_1$ ).

For some reason that will be clarified later, we would like to enlarge the admissible function set  $\mathcal{X}$ , allowing functions to be discontinuous at  $\Gamma_c$ . In this context, it is clear that the variational formulation (1) makes no sense and must be altered in order to ensure that the solution of this extended problem responds to the same Euler equations that those of the original problem. The idea behind this modified variational formulation is to incorporate additional terms based on the virtual power performed by the discontinuities of the unknowns on the interface. More precisely, let  $\mathcal{X}_d = \mathcal{X}_1 \times \mathcal{X}_2$  where  $\mathcal{X}_1 = \{\theta_1 \in H^1(\Omega_1); \theta_1 = \bar{\theta}_{|\Gamma_{1D}} \text{ on } \Gamma_{1D}\}$  and  $\mathcal{X}_2 = \{\theta_2 \in H^1(\Omega_2); \theta_2 = \bar{\theta}_{|\Gamma_{2D}} \text{ on } \Gamma_{2D}\}$ . Observe that  $\mathcal{X}_d$  is a larger set, i.e.,  $\mathcal{X} \subset \mathcal{X}_d$ . We also introduce variables  $r_1 \in \mathcal{Z}_1, r_2 \in \mathcal{Z}_2$ , being  $\mathcal{Z}_1$  and  $\mathcal{Z}_2$  proper function sets. In this particular case  $\mathcal{Z}_1 = \mathcal{Z}_2 = H^{-1/2}(\Gamma_c)$ . Index  $i$  will correspond to part  $\Omega_i, i = 1, 2$ . Then, there exists a  $\gamma$ -family of equivalent variational formulations for the extended problem that reads as follows: *for some  $\gamma \in [0, 1]$ , find  $(\theta, r_1, r_2) \in \mathcal{X}_d \times \mathcal{Z}_1 \times \mathcal{Z}_2$  such that*

$$\begin{aligned} & \int_{\Omega_1} k\nabla\theta_1 \cdot \nabla\eta_1 \, d\mathbf{x} + \int_{\Omega_2} k\nabla\theta_2 \cdot \nabla\eta_2 \, d\mathbf{x} \\ & + \gamma \int_{\Gamma_c} r_1(\eta_1 - \eta_2) \, d\Gamma + (1 - \gamma) \int_{\Gamma_c} r_2(\eta_1 - \eta_2) \, d\Gamma \\ & + \gamma \int_{\Gamma_c} s_1(\theta_1 - \theta_2) \, d\Gamma + (1 - \gamma) \int_{\Gamma_c} s_2(\theta_1 - \theta_2) \, d\Gamma \\ & = \int_{\Omega_1} f\eta_1 \, d\mathbf{x} + \int_{\Omega_2} f\eta_2 \, d\mathbf{x} \quad \forall (\eta, s_1, s_2) \in \mathcal{Y}_d \times \mathcal{Z}_1 \times \mathcal{Z}_2, \end{aligned} \quad (3)$$

with  $\eta = (\eta_1, \eta_2) \in \mathcal{Y}_d$  the admissible variations of functions in  $\mathcal{X}_d$  given by

$$\begin{aligned}\mathcal{Y}_d &= \mathcal{Y}_1 \times \mathcal{Y}_2, \\ \mathcal{Y}_1 &= \{\eta_1 \in H^1(\Omega_1); \eta_1 = 0 \text{ on } \Gamma_{1D}\}, \\ \mathcal{Y}_2 &= \{\eta_2 \in H^1(\Omega_2); \eta_2 = 0 \text{ on } \Gamma_{2D}\}.\end{aligned}\tag{4}$$

It is readily verified that the Euler equations and the Weierstrass–Erdmann corner conditions associated to the family of variational formulations (3), just in terms of  $\theta$ , are the following

$$\begin{cases} -k\Delta\theta_1 = f & \text{in } \Omega_1, \\ -k\Delta\theta_2 = f & \text{in } \Omega_2, \\ k\nabla\theta_1 \cdot \mathbf{n}_{c1} = k\nabla\theta_2 \cdot \mathbf{n}_{c1} & \text{on } \Gamma_c, \\ \theta_1 = \theta_2 & \text{on } \Gamma_c, \end{cases}\tag{5}$$

where  $r_\gamma = \gamma r_1 + (1-\gamma)r_2 = -k\nabla\theta_1 \cdot \mathbf{n}_{c1} = -k\nabla\theta_2 \cdot \mathbf{n}_{c1}$ . Observe that the solution of the variational problem (3) satisfies the same Euler equations that the variational problem (1). In this way it is possible, from a variational context, to recover information of the original problem without imposing conditions or restrictions over function sets  $\mathcal{X}_1$  and  $\mathcal{X}_2$  at  $\Gamma_c$ . The advantage here is the arbitrariness in choosing sets  $\mathcal{X}_1$  and  $\mathcal{X}_2$ .

**Remark 1** *On one hand, problem (3) resembles those variational formulations derived from domain decomposition techniques [5]. Indeed, the present approach may be regarded as a generalization, since by taking  $r_\gamma = \gamma r_1 + (1-\gamma)r_2$  as a unique variable within the problem we recover those methods. On the other hand, by taking  $\gamma = \frac{1}{2}$  we recover another class of formulations arising when minimizing relaxed functionals [8].*

**Remark 2** *Notice that, for any associated discrete problem, formulation (3) allows us to consider non-matching meshes for domains  $\Omega_i$ ,  $i = 1, 2$  at both sides of the internal boundary  $\Gamma_c$ . In this case  $r_1$  and  $r_2$  may pertain to different finite-dimensional spaces. Therefore, for each value of  $\gamma$ , the sense in which the Euler equations are satisfied is strongly related to the characteristics of each mesh.*

In anticipation of treating the coupling problem between hemodynamics models of different dimensionality, we will present at this stage the simple case of coupling 3D–1D models for the heat transfer equations. This situation can be thought of as a problem where discontinuous fields arise due to the difference in the *kinematics* assumed for different parts of the domain.

Let us consider the particular situation exposed in Figure 2 for which we have  $\Gamma = \Gamma_A \cup \Gamma_{L_1} \cup \Gamma_{L_2} \cup \Gamma_B$ , with essential boundary conditions over  $\Gamma_A$  and  $\Gamma_B$ , namely  $\bar{\theta}_A$  and  $\bar{\theta}_B$ , and with homogeneous Neumann boundary condition over  $\Gamma_{L_1} \cup \Gamma_{L_2}$ .

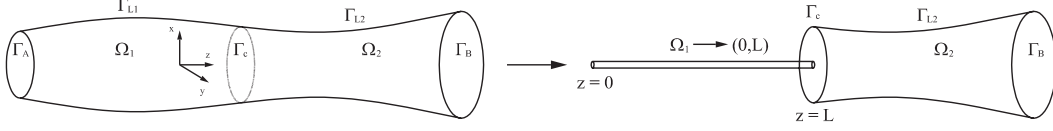


Fig. 2. Coupling 3D–1D models for the heat transfer problem.

In the extended variational formulation (3) we assume the temperature  $\theta_1$  to be constant along each transversal section with respect to the axial direction  $\mathbf{e}_z$ . That is,  $\theta_{|\Omega_1} = \theta_1(z)$  where  $z$  is the coordinate over  $\mathbf{e}_z$  axis. Consequently we denote with  $\eta_1(z)$  the admissible variations of the temperature in  $\Omega_1$ . We also consider  $r_1$  constant on  $\Gamma_c$ . With these assumptions it is possible to integrate along the transversal section and to write a reduced 1D model achieving the following problem: *for some  $\gamma \in [0, 1]$ , find  $(\theta_1, \theta_2, r_1, r_2) \in \mathcal{X}_d \times \mathcal{Z}_1 \times \mathcal{Z}_2$  such that*

$$\begin{aligned} & \int_0^L A(z)k \frac{\partial \theta_1}{\partial z} \frac{\partial \eta_1}{\partial z} dz + \int_{\Omega_2} k \nabla \theta_2 \cdot \nabla \eta_2 dx \\ & \quad + \gamma \int_{\Gamma_c} r_1 (\eta_1 - \eta_2) d\Gamma + (1 - \gamma) \int_{\Gamma_c} r_2 (\eta_1 - \eta_2) d\Gamma \\ & \quad + \gamma \int_{\Gamma_c} s_1 (\theta_1 - \theta_2) d\Gamma + (1 - \gamma) \int_{\Gamma_c} s_2 (\theta_1 - \theta_2) d\Gamma \\ & = \int_0^L \bar{f} \eta_1 dz + \int_{\Omega_2} f \eta_2 dx \quad \forall (\eta_1, \eta_2, s_1, s_2) \in \mathcal{Y}_d \times \mathcal{Z}_1 \times \mathcal{Z}_2, \end{aligned} \quad (6)$$

where  $\bar{f} = \int_{\Gamma_z} f d\Gamma$  over each transversal section. In this particular case it is easy to see that, being  $\mathcal{X}_d = \mathcal{X}_1 \times \mathcal{X}_2$ , we have

$$\begin{aligned} \mathcal{X}_1 &= \{\theta_1 \in H^1(0, L); \theta_1 = \bar{\theta}_A \text{ in } z = 0\}, \\ \mathcal{X}_2 &= \{\theta_2 \in H^1(\Omega_2); \theta_2 = \bar{\theta}_B \text{ on } \Gamma_B\}, \\ \mathcal{Z}_1 &= \mathbb{R}, \\ \mathcal{Z}_2 &= H^{-1/2}(\Gamma_c). \end{aligned} \quad (7)$$

In the following we give the main steps in proving the existence and uniqueness of the solution. Firstly, the existence and uniqueness of the solution  $\theta = (\theta_1, \theta_2)$  is straightforwardly proved by using the theory of elliptic problems [5,12], for which we have to work with the kernel of the operator  $\mathcal{B}$  (associated to the bilinear form  $b(\cdot, \cdot)$  corresponding to the equation of  $r_\gamma = \gamma r_1 + (1 - \gamma)r_2$ ), that is a subspace of  $\mathcal{X}_d$ . Indeed, let  $\mathcal{W}_d = H^1(0, L) \times H^1(\Omega_2)$  equipped with the norm  $\|\theta\|_{\mathcal{W}_d} = \|\theta_1\|_{H^1(0,L)} + \|\theta_2\|_{H^1(\Omega_2)}$  and consider the following decomposition  $\theta = \mu + \xi$  where  $\xi \in \mathcal{W}_d$  is such that  $\xi_1(0) = \bar{\theta}_A$ ,  $\xi_1(L) = 0$  and  $\xi_2|_{\Gamma_B} = \bar{\theta}_B$ ,  $\xi_2|_{\Gamma_A} = 0$ , while  $\mu \in \mathcal{K}_\gamma \subset \text{Ker}(\mathcal{B})$  being

$$\begin{aligned} \mathcal{K}_\gamma &= \left\{ \mu = (\mu_1, \mu_2) \in \mathcal{W}_d; \mu_1(0) = 0, \mu_2|_{\Gamma_B} = 0, \right. \\ & \quad \left. \gamma \left[ \mu_1(L) - \frac{1}{A_c} \int_{\Gamma_c} \mu_2 d\Gamma \right] = 0, (1 - \gamma)[\mu_1(L) - \mu_2|_{\Gamma_c}] = 0 \right\}. \end{aligned} \quad (8)$$

Consider the bilinear form  $a : \mathcal{K}_\gamma \times \mathcal{K}_\gamma \rightarrow \mathbb{R}$

$$a(\mu, \eta) = \int_0^L Ak \frac{\partial \mu_1}{\partial z} \frac{\partial \eta_1}{\partial z} dz + \int_{\Omega_2} k \nabla \mu_2 \cdot \nabla \eta_2 dx, \quad (9)$$

that is trivially symmetric, continuous and coercive in  $\mathcal{K}_\gamma \times \mathcal{K}_\gamma$  provided  $A \in L^\infty(0, L)$  and  $A \geq A_o > 0$ ,  $k \geq k_o > 0$  in  $(0, L)$  (that is always satisfied). Consider the linear functional  $l : \mathcal{K}_\gamma \rightarrow \mathbb{R}$  given by

$$l(\eta) = \int_0^L \bar{f} \eta_1 dz + \int_{\Omega_2} f \eta_2 dx, \quad (10)$$

that is obviously continuous in  $\mathcal{K}_\gamma$  provided  $\bar{f} \in H^{-1}(0, L)$  and  $f \in H^{-1}(\Omega_2)$ . Then, by the Lax–Milgram theorem there exists a unique solution  $\mu \in \mathcal{K}_\gamma \subset \text{Ker}(\mathcal{B})$  such that

$$a(\mu, \eta) = \tilde{l}(\eta) \quad \forall \eta \in \mathcal{K}_\gamma, \quad (11)$$

where  $\tilde{l}(\eta) = l(\eta) - a(\xi, \eta)$ . Therefore, the existence and uniqueness of  $\theta = (\theta_1, \theta_2)$ , solution of problem (19) follow. To prove the existence and uniqueness of  $r_\gamma \in H_{[\cdot]}^{-1/2}(\Gamma_c)$ , we need to resort to the theory of mixed problems [5,12]. In this case we have a classical mixed problem with a bilinear form  $b : \mathcal{Y}_d \times H_{[\cdot]}^{-1/2}(\Gamma_c) \rightarrow \mathbb{R}$  given by

$$b(\mu, r_\gamma) = \int_{\Gamma_c} r_\gamma (\mu_1 - \mu_2) d\Gamma. \quad (12)$$

Since the bilinear form  $b(\cdot, \cdot)$  satisfies the corresponding inf–sup condition, i.e. the existence of  $\beta_0 > 0$  such that

$$\beta_0 \leq \inf_{\substack{r_\gamma \in H_{[\cdot]}^{-1/2}(\Gamma_c) \\ r_\gamma \neq 0}} \sup_{\substack{\psi \in \mathcal{W}_d \\ \llbracket \mu \rrbracket = \psi_1(L) - \psi_2|_{\Gamma_c} \\ \psi_1(L) \neq \psi_2|_{\Gamma_c}}} \frac{\int_{\Gamma_c} r_\gamma \llbracket \mu \rrbracket d\Gamma}{\|\psi\|_{\mathcal{W}_d} \|r_\gamma\|_{H_{[\cdot]}^{-1/2}(\Gamma_c)}}, \quad (13)$$

then there exists a unique  $r_\gamma \in H_{[\cdot]}^{-1/2}(\Gamma_c)$  solution of problem (6). It remains to see (13). Observe that  $H_{[\cdot]}^{-1/2}(\Gamma_c)$ , endowed with the norm

$$\|r_\gamma\|_{H_{[\cdot]}^{-1/2}(\Gamma_c)} = \sup_{\substack{\llbracket \mu \rrbracket \in H_{[\cdot]}^{1/2}(\Gamma_c) \\ \llbracket \mu \rrbracket \neq 0}} \frac{\int_{\Gamma_c} r_\gamma \llbracket \mu \rrbracket d\Gamma}{\|\llbracket \mu \rrbracket\|_{H_{[\cdot]}^{1/2}(\Gamma_c)}}, \quad (14)$$

is the dual space of  $H_{[\cdot]}^{1/2}(\Gamma_c)$  defined by

$$H_{[\cdot]}^{1/2}(\Gamma_c) = \{\llbracket \mu \rrbracket \in H^{1/2}(\Gamma_c); \mu \in \mathcal{W}_d; \llbracket \mu \rrbracket = \mu_1(L) - \mu_2|_{\Gamma_c}\}, \quad (15)$$

equipped with the norm

$$\|[\mu]\|_{H_{[\cdot]}^{1/2}(\Gamma_c)} = \inf_{\substack{\varphi \in \mathcal{W}_d \\ [\mu] = \varphi_1(L) - \varphi_2|_{\Gamma_c}}} \|\varphi\|_{\mathcal{W}_d}. \quad (16)$$

Thus, for any  $\beta_1 > 1$  we can choose  $\psi$  such that  $\psi_1(L) - \psi_2|_{\Gamma_c} = [\mu]$  and

$$\|\psi\|_{\mathcal{W}_d} \leq \beta_1 \|[\mu]\|_{H_{[\cdot]}^{1/2}(\Gamma_c)}. \quad (17)$$

From definition (14), and using (17) we have for  $\beta_2 > 1$  the following

$$\frac{1}{\beta_2} \|r_\gamma\|_{H_{[\cdot]}^{-1/2}(\Gamma_c)} < \sup_{\substack{[\mu] \in H_{[\cdot]}^{1/2}(\Gamma_c) \\ [\mu] \neq 0}} \frac{\int_{\Gamma_c} r_\gamma [\mu] \, d\Gamma}{\|[\mu]\|_{H_{[\cdot]}^{1/2}(\Gamma_c)}} \leq \beta_1 \sup_{\substack{\psi \in \mathcal{W}_d \\ [\mu] = \psi_1(L) - \psi_2|_{\Gamma_c} \\ \psi_1(L) \neq \psi_2|_{\Gamma_c}}} \frac{\int_{\Gamma_c} r_\gamma [\mu] \, d\Gamma}{\|\psi\|_{\mathcal{W}_d}}, \quad (18)$$

and (13) follows with  $\beta_0 = \frac{1}{\beta_1 \beta_2} > 0$ .

It is worthwhile to show the consequences of considering different values of  $\gamma$  for this particular case. The general situation gives, from variational formulation (6), the following Euler equations and Weierstrass–Erdmann corner conditions

$$\begin{cases} -k \frac{\partial}{\partial z} \left( A(z) \frac{\partial \theta_1}{\partial z} \right) = \bar{f} & \text{in } (0, L), \\ -k \Delta \theta_2 = f & \text{in } \Omega_2, \\ k \nabla \theta_2 \cdot \mathbf{n}_2 = 0 & \text{on } \Gamma_{L_2}, \\ -k \frac{\partial \theta_1}{\partial z} = \gamma r_1 + (1 - \gamma) \frac{1}{A_c} \int_{\Gamma_c} r_2 \, d\Gamma & \text{in } z = L, \\ -k \nabla \theta_2 \cdot \mathbf{n}_1 = \gamma r_1 + (1 - \gamma) r_2 & \text{on } \Gamma_c, \\ \gamma \left[ \theta_1 - \frac{1}{A_c} \int_{\Gamma_c} \theta_2 \, d\Gamma \right] = 0 & \text{in } z = L, \\ (1 - \gamma) [\theta_1 - \theta_2] = 0 & \text{on } \Gamma_c. \end{cases} \quad (19)$$

Observe now that the value of  $\gamma$  is important since it determines the sense in which equations (19) are satisfied. For example with  $\gamma = 1$  we have the following problem

$$\begin{cases} -k \frac{\partial}{\partial z} \left( A(z) \frac{\partial \theta_1}{\partial z} \right) = \bar{f} & \text{in } (0, L), \\ -k \Delta \theta_2 = f & \text{in } \Omega_2, \\ k \nabla \theta_2 \cdot \mathbf{n}_2 = 0 & \text{on } \Gamma_{L_2}, \\ k \frac{\partial \theta_1}{\partial z} = k \nabla \theta_2 \cdot \mathbf{n}_1 & \text{on } \Gamma_c, \\ \theta_1 = \frac{1}{A_c} \int_{\Gamma_c} \theta_2 \, d\Gamma & \text{in } z = L. \end{cases} \quad (20)$$

The above set of equations can be interpreted, roughly speaking, as a problem in which the 1D model feeds the 3D model with a constant Neumann boundary condition (equation (20)<sub>4</sub>), while the 3D model provides the 1D model with a Dirichlet boundary condition (equation (20)<sub>5</sub>). Notice that for this situation we have  $r_1 = -k \frac{\partial \theta_1}{\partial z}(L) = -k(\nabla \theta_2 \cdot \mathbf{n}_1)|_{\Gamma_c}$ , and hence  $\nabla \theta_2 \cdot \mathbf{n}_1$  is constant on  $\Gamma_c$ .

The case  $\gamma = 0$  leads to

$$\begin{cases} -k \frac{\partial}{\partial z} \left( A(z) \frac{\partial \theta_1}{\partial z} \right) = \bar{f} & \text{in } (0, L), \\ -k \Delta \theta_2 = f & \text{in } \Omega_2, \\ k \nabla \theta_2 \cdot \mathbf{n}_2 = 0 & \text{on } \Gamma_{L_2}, \\ k \frac{\partial \theta_1}{\partial z} = \frac{1}{A_c} \int_{\Gamma_c} k \nabla \theta_2 \cdot \mathbf{n}_1 \, d\Gamma & \text{in } z = L, \\ \theta_1 = \theta_2 & \text{on } \Gamma_c. \end{cases} \quad (21)$$

Contrariwise, this problem can be viewed, again roughly speaking, as a situation where the 1D model furnishes the 3D model with a constant Dirichlet boundary condition (equation (21)<sub>5</sub>), while the 3D model feeds the 1D model with a Neumann boundary condition (equation (21)<sub>4</sub>). In this case we have  $r_2 = -k(\nabla \theta_2 \cdot \mathbf{n}_1)|_{\Gamma_c}$  and  $-k \frac{\partial \theta_1}{\partial z}(L) = \frac{1}{A_c} \int_{\Gamma_c} r_2 \, d\Gamma$ .

Observe that there exists a reciprocity relationship between cases at both extreme values of  $\gamma$ . In effect, for the case  $\gamma = 0$  we obtain a situation in which the continuity in  $\theta$  is actually enforced in a point-wise sense. As a counterpart we only recover the continuity of the mean value for the heat flow (see equation (21)<sub>4</sub>). Conversely, with  $\gamma = 1$  we have ensured the continuity for the heat flux in a point-wise sense, while in this case we only recover the continuity for the mean value of the temperature (see equation (20)<sub>5</sub>). Nonetheless, in spite of the differences commented, we see that always we attain a well-posed problem for any choice of  $\gamma$ . That is, we can go from a pure Dirichlet (Neumann) problem, with  $\gamma = 0$ , to a pure Neumann (Dirichlet) problem, with  $\gamma = 1$ , concerning the 3D domain (1D domain).

The opposite situations referred to in the above arise only in the particular case when a kinematical assumption over a portion of the domain  $\Omega$  has been considered. In the case of no kinematical constraints, as the situation given by problem (3), we do not discern this reciprocity, and the kinematical restrictions appear only at the discrete counterpart of the problem when the corresponding, possibly non-matching, discretizations for  $\Omega_1$  and  $\Omega_2$  are given.

### 3 Variational formulation for fluid flow in compliant vessels

In this section we address the problem of the flow of an incompressible fluid within a compliant domain.

Let us consider an arbitrary compliant vessel given by the domain  $\Omega \subset \mathbb{R}^{n_d}$ , ( $n_d = 2, 3$ ) as shown in Figure 3 with boundary  $\Gamma$  decomposed in the part corresponding to the wall, namely  $\Gamma_w$ , and the corresponding ones to each input–output face, namely  $\Gamma_i$ . Thus we have  $\Gamma = \Gamma_w \cup \left(\bigcup_{i=1}^{N_s} \Gamma_i\right)$ , where  $N_s$  is the total number of faces for which we have interchange of mass by setting corresponding Dirichlet conditions. Let us suppose a no–slip condition over  $\Gamma_w$ , even so, we consider the corresponding traction over  $\Gamma_w$  that accomplishes the equilibrium. This traction will be given consistent with the structural model. The problem can be stated in an Eulerian framework, or in an arbitrary Lagrangian–Eulerian framework as well [16].

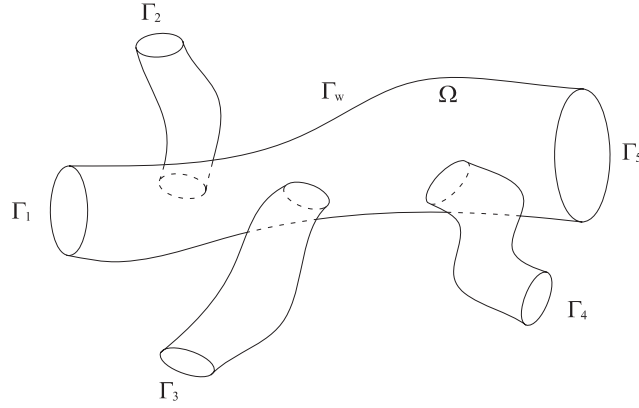


Fig. 3. Arbitrary compliant vessel.

Within the context of an ALE variational approach, the flow of an incompressible fluid in a compliant vessel, like the one shown in Figure 3, can be formulated as follows: *for every  $t \in (0, T)$ , find  $(\mathbf{u}, p) \in \mathcal{U} \times \mathcal{P}$  such that*

$$\begin{aligned} \int_{\Omega} \rho \frac{\partial \mathbf{u}}{\partial t} \Big|_{\mathbf{Y}} \cdot \mathbf{v} \, d\mathbf{x} + \int_{\Omega} \rho \nabla \mathbf{u} (\mathbf{u} - \mathbf{w}) \cdot \mathbf{v} \, d\mathbf{x} \\ - \int_{\Omega} p \operatorname{div} \mathbf{v} \, d\mathbf{x} + \int_{\Omega} \boldsymbol{\sigma}_D(\mathbf{u}) \cdot \boldsymbol{\varepsilon}(\mathbf{v}) \, d\mathbf{x} - \int_{\Omega} \mathbf{f} \cdot \mathbf{v} \, d\mathbf{x} \\ - \int_{\Gamma_w} \mathbf{t}_w \cdot \mathbf{v} \, d\Gamma = 0 \quad \forall \mathbf{v} \in \mathcal{V}, \end{aligned} \quad (22a)$$

$$\int_{\Omega} \rho \operatorname{div} \mathbf{u} \, q \, d\mathbf{x} = 0 \quad \forall q \in \mathcal{Q}, \quad (22b)$$

with proper initial conditions. Here,  $\mathbf{u}$  is the velocity field,  $\mathbf{v}$  is an admissible variation of the velocity field,  $\mathbf{w}$  is the velocity of the ALE frame of reference,  $\boldsymbol{\sigma} = -p\mathbf{I} + \boldsymbol{\sigma}_D(\mathbf{u})$  is the Cauchy stress tensor where  $p$  is the pressure field and  $\boldsymbol{\sigma}_D(\mathbf{u})$  is its deviatoric part,  $q$  is an admissible variation of the pressure

field,  $\rho$  is the fluid density,  $\mathbf{f}$  is a volume force,  $\mathbf{t}_w$  is the traction vector over the vessel wall,  $\mathbf{n}$  is the corresponding outward unit normal vector and  $\boldsymbol{\varepsilon}(\mathbf{v})$  is the strain rate tensor associated to the admissible variation  $\mathbf{v}$ . Also,  $\frac{\partial(\cdot)}{\partial t}\Big|_{\mathbf{Y}}$  denotes the derivative when fixing ALE coordinates  $\mathbf{Y}$ , also  $\mathbf{f}$  and  $\mathbf{t}_w$  are such that expression (22a) makes sense. After a little of calculus it is possible to obtain a conservative form for the mass conservation equation as follows

$$\frac{d}{dt} \int_{\Omega} \rho q \, d\mathbf{x} - \int_{\Omega} \rho(\mathbf{u} - \mathbf{w}) \cdot \nabla q \, d\mathbf{x} + \int_{\Gamma} \rho(\mathbf{u} - \mathbf{w}) \cdot \mathbf{n} q \, d\Gamma = 0 \quad \forall q \in \mathcal{Q}. \quad (23)$$

In this problem we consider null mass flux across the vessel wall  $\Gamma_w$ .

The set  $\mathcal{U} \times \mathcal{P}$  establishes regularity and essential boundary conditions such that problem (22) is well-posed. Therefore, variational formulation (22) is well stated only when working with fields  $(\mathbf{u}, p)$  being regular enough in  $\Omega$ , in the sense that the pair must be in  $\mathcal{U} \times \mathcal{P}$ . It is usual to consider for formulation (23) that

$$\begin{aligned} \mathcal{U} &= \{\mathbf{u} \in [H^1(\Omega)]^{n_d}; \mathbf{u}|_{\Gamma_i} = \bar{\mathbf{u}}_i \text{ on } \Gamma_i, i = 1, \dots, N_s\}, \\ \mathcal{P} &= L^2(\Omega), \end{aligned} \quad (24)$$

while we demand additional regularity for field  $p$  if we work with the conservative form of the mass conservation given by (23).

So far it was not specified how the vessel wall responds to fluid stresses. At this moment it is assumed that there exists a model for the wall that takes into account the fluid–structure interaction problem by means of a traction vector  $\mathbf{t}_w$  such that a no–slip condition over  $\Gamma_w$  is accomplished.

#### 4 Extended variational formulation for fluid flow in compliant vessels

In order to recast the problem of coupling 3D with 1D models for modelling the blood flow in large arteries we turn to introducing different kinematics for each part of a given domain, that will correspond to the 3D and 1D models. In this sense, we interpret that discontinuities may occur at the coupling interface as a result of the dissimilarity between the kinematics of each model, in the same way as done in the heat transfer problem. The goal of this section is to introduce an extended governing variational principle that allows us to establish different kinematics for different parts of a given split domain, and thus to manage the mentioned discontinuities in the involved fields.

#### 4.1 Statement of the problem

For the sake of simplicity in illustrating the problem we work with the simple domain already shown in Figure 2. Recall that  $\Gamma_c$  is an internal boundary of  $\Omega$  that splits the domain as being  $\Omega = \Omega_1 \cup \Omega_2 \cup \Gamma_c$ , with boundaries  $\Gamma_1$  and  $\Gamma_2$  respectively. Thus, we have  $\Gamma_c = \Gamma_1 \cap \Gamma_2$ . The vessel wall is now decomposed as  $\Gamma_w = \Gamma_{w1} \cup \Gamma_{w2}$ , and we also refer to  $\Gamma_A$  and  $\Gamma_B$  as  $\Gamma_{\text{in}}$  and  $\Gamma_{\text{out}}$  respectively. Then we have  $\Gamma_1 = \Gamma_{\text{in}} \cup \Gamma_{w1} \cup \Gamma_c$  and  $\Gamma_2 = \Gamma_{\text{out}} \cup \Gamma_{w2} \cup \Gamma_c$ . As mentioned, we will work with different kinematics on each part of  $\Omega$ , say  $\Omega_1$  and  $\Omega_2$ , proceeding analogously to that performed for the heat transfer problem.

We shall also suppose, without loss of generality, that the problem is such that has proper Dirichlet boundary conditions at both extremes of domain  $\Omega$ , that is at  $\Gamma_{\text{in}}$  and  $\Gamma_{\text{out}}$ . In this way, the analysis will be focused where discontinuities occur, that is on  $\Gamma_c$ .

Let us consider over  $\Omega_i$  function set  $\mathcal{U}_i \times \mathcal{P}_i$ ,  $i = 1, 2$ , that will characterize the corresponding model. No assumptions are made concerning conditions at interface  $\Gamma_c$ . Let us take the velocity  $\mathbf{w}$  of the ALE frame of reference such that  $\mathbf{w} \cdot \mathbf{n} = 0$  on  $\Gamma_{\text{in}}$ ,  $\Gamma_{\text{out}}$  and  $\Gamma_c$ . With regards to traction  $\mathbf{t}_w$ , it will be given such that  $\mathbf{u} = \mathbf{w}$  on  $\Gamma_w = \Gamma_{w1} \cup \Gamma_{w2}$ . Although we have presented the general problem with a Neumann boundary condition over  $\Gamma_w$ , observe that it would be equivalent if we consider a no-slip condition over such a portion of the boundary.

Let us write  $\mathbf{u} = (\mathbf{u}_1, \mathbf{u}_2)$ , with  $\mathbf{u}_1 \in \mathcal{U}_1$  and  $\mathbf{u}_2 \in \mathcal{U}_2$ . In the same way it is  $p = (p_1, p_2)$  with  $p_1 \in \mathcal{P}_1$  and  $p_2 \in \mathcal{P}_2$ . Then we have  $\mathcal{U}_d = \mathcal{U}_1 \times \mathcal{U}_2$  and  $\mathcal{P}_d = \mathcal{P}_1 \times \mathcal{P}_2$ . We will focus our attention upon the momentum equation. Thus, the resulting extended variational principle for the momentum balance, written in a total Eulerian form in domain  $\Omega_1$ , is the following

$$\begin{aligned}
& \int_{\Omega_1} \rho \frac{\partial \mathbf{u}_1}{\partial t} \cdot \mathbf{v}_1 \, d\mathbf{x} + \int_{\Omega_1} \rho (\nabla \mathbf{u}_1) \mathbf{u}_1 \cdot \mathbf{v}_1 \, d\mathbf{x} \\
& - \int_{\Omega_1} p_1 \operatorname{div} \mathbf{v}_1 \, d\mathbf{x} + \int_{\Omega_1} \boldsymbol{\sigma}_D(\mathbf{u}_1) \cdot \boldsymbol{\varepsilon}(\mathbf{v}_1) \, d\mathbf{x} - \int_{\Omega_1} \mathbf{f} \cdot \mathbf{v}_1 \, d\mathbf{x} - \int_{\Gamma_{w1}} \mathbf{t}_w \cdot \mathbf{v}_1 \, d\Gamma \\
& \quad + \int_{\Omega_2} \rho \frac{\partial \mathbf{u}_2}{\partial t} \Big|_{\mathbf{Y}} \cdot \mathbf{v}_2 \, d\mathbf{x} + \int_{\Omega_2} \rho \nabla \mathbf{u}_2 (\mathbf{u}_2 - \mathbf{w}) \cdot \mathbf{v}_2 \, d\mathbf{x} \\
& - \int_{\Omega_2} p_2 \operatorname{div} \mathbf{v}_2 \, d\mathbf{x} + \int_{\Omega_2} \boldsymbol{\sigma}_D(\mathbf{u}_2) \cdot \boldsymbol{\varepsilon}(\mathbf{v}_2) \, d\mathbf{x} - \int_{\Omega_2} \mathbf{f} \cdot \mathbf{v}_2 \, d\mathbf{x} - \int_{\Gamma_{w2}} \mathbf{t}_w \cdot \mathbf{v}_2 \, d\Gamma \\
& + \int_{\Gamma_c} [\gamma \mathbf{r}_1 + (1 - \gamma) \mathbf{r}_2] \cdot (\mathbf{v}_2 - \mathbf{v}_1) \, d\Gamma + \int_{\Gamma_c} [\gamma \mathbf{s}_1 + (1 - \gamma) \mathbf{s}_2] \cdot (\mathbf{u}_2 - \mathbf{u}_1) \, d\Gamma = 0 \\
& \quad \forall (\mathbf{v}, \mathbf{s}_1, \mathbf{s}_2) \in \mathcal{V}_d \times \mathcal{Z}_1 \times \mathcal{Z}_2, \quad (25)
\end{aligned}$$

where  $\mathbf{r}_1 \in \mathcal{Z}_1$  and  $\mathbf{r}_2 \in \mathcal{Z}_2$  are the counterpart variables of  $r_1$  and  $r_2$  present in the heat transfer problem, with variations  $\mathbf{s}_1$  and  $\mathbf{s}_2$  respectively. Also we

have  $\mathbf{v} = (\mathbf{v}_1, \mathbf{v}_2) \in \mathcal{V}_d = \mathcal{V}_1 \times \mathcal{V}_2$ .

Notice that formulation (25) could have also been generalized for the situation with several faces  $\Gamma_{ci}$ ,  $i = 1, \dots, N_c$  where discontinuities can occur. This generalization is straightforward and was omitted here for the sake of brevity.

Now let us suppose that fields  $\mathbf{u}_1$ ,  $p_1$  and  $\mathbf{r}_1$  over  $\Omega_1$  and  $\Gamma_c$  respectively are given by the following particular forms

$$\begin{aligned}\mathbf{u}_1 &= \bar{u}(z, t)\mathbf{e}_z, \\ p_1 &= \bar{p}(z, t), \\ \mathbf{r}_1 &= \bar{r}_1(t)\mathbf{e}_z,\end{aligned}\tag{26}$$

where  $\mathbf{e}_z$  is the unit axial vector in the direction of the normal to a generic transversal plane defined by coordinates  $x, y$  (see Figure 2).

Therefore, introducing assumptions (26) into expression (25), integrating over the transversal area  $\Gamma_z$ , namely  $A(z, t)$ , considering the corresponding form of the admissible variations and assuming that there is no elongation of the domain in the  $\mathbf{e}_z$  direction we obtain, after a little of work, the following expression

$$\begin{aligned}& \int_0^L \rho A \frac{\partial \bar{u}}{\partial t} \bar{v} \, dz + \int_0^L \rho A \bar{u} \frac{\partial \bar{u}}{\partial z} \bar{v} \, dz - \int_0^L A \bar{p} \frac{\partial \bar{v}}{\partial z} \, dz + \int_0^L \bar{\boldsymbol{\sigma}}(\bar{u}) \cdot (\mathbf{e}_z \otimes \mathbf{e}_z) \frac{\partial \bar{v}}{\partial z} \, dz \\ & \quad - \int_0^L \oint_{C_z} t_w^z \bar{v} \, dl \, dz - \int_0^L f^z \bar{v} \, dz \\ & \quad + \int_{\Omega_2} \rho \frac{\partial \mathbf{u}_2}{\partial t} \Big|_{\mathbf{Y}} \cdot \mathbf{v}_2 \, d\mathbf{x} + \int_{\Omega_2} \rho \nabla \mathbf{u}_2 (\mathbf{u}_2 - \mathbf{w}) \cdot \mathbf{v}_2 \, d\mathbf{x} \\ & - \int_{\Omega_2} p_2 \operatorname{div} \mathbf{v}_2 \, d\mathbf{x} + \int_{\Omega_2} \boldsymbol{\sigma}_D(\mathbf{u}_2) \cdot \boldsymbol{\varepsilon}(\mathbf{v}_2) \, d\mathbf{x} - \int_{\Omega_2} \mathbf{f} \cdot \mathbf{v}_2 \, d\mathbf{x} - \int_{\Gamma_{w2}} \mathbf{t}_w \cdot \mathbf{v}_2 \, d\Gamma \\ & \quad + \int_{\Gamma_c} [\gamma \bar{r}_1 (\mathbf{v}_2 \cdot \mathbf{n}_1 - \bar{v}) + (1 - \gamma) \mathbf{r}_2 \cdot (\mathbf{v}_2 - \bar{v} \mathbf{n}_1)] \, d\Gamma \\ & \quad + \int_{\Gamma_c} [\gamma \bar{s}_1 (\mathbf{u}_2 \cdot \mathbf{n}_1 - \bar{u}) + (1 - \gamma) \mathbf{s}_2 \cdot (\mathbf{u}_2 - \bar{u} \mathbf{n}_1)] \, d\Gamma = 0\end{aligned}$$

$$\forall (\mathbf{v}, \mathbf{s}_1, \mathbf{s}_2) \in \mathcal{V}_d \times \mathcal{Z}_1 \times \mathcal{Z}_2, \tag{27}$$

where  $f^z = \int_{\Gamma_z} \mathbf{f} \cdot \mathbf{e}_z \, d\Gamma$ ,  $\bar{\boldsymbol{\sigma}}_D(\bar{u}) = \int_{\Gamma_z} \boldsymbol{\sigma}_D(\bar{u}) \, d\Gamma$ ,  $C_z$  is the boundary curve of the generic transversal section  $A(z, t)$  and  $t_w^z$  is the component of  $\mathbf{t}_w$  in the  $\mathbf{e}_z$  direction. Also notice that over  $\Gamma_c$  we have  $\mathbf{e}_z = \mathbf{n}_1 = -\mathbf{n}_2$ . It is not difficult to see that

$$\oint_{C_z} t_w^z \, dl = \bar{p} \frac{\partial A}{\partial z} - \oint_{C_z} \boldsymbol{\sigma}_D(\bar{u}) \cdot (\mathbf{e}_z \otimes \mathbf{n}_w) \, dl, \tag{28}$$

where  $\mathbf{n}_w$  is the outward unit normal vector of the boundary corresponding

to the wall  $\Gamma_{w_1}$ . Introducing this expression in equation (27) follows that

$$\begin{aligned}
& \int_0^L \rho A \frac{\partial \bar{u}}{\partial t} \bar{v} \, dz + \int_0^L \rho A \bar{u} \frac{\partial \bar{v}}{\partial z} \, dz - \int_0^L A \bar{p} \frac{\partial \bar{v}}{\partial z} \, dz + \int_0^L \bar{\boldsymbol{\sigma}}(\bar{u}) \cdot (\mathbf{e}_z \otimes \mathbf{e}_z) \frac{\partial \bar{v}}{\partial z} \, dz \\
& - \int_0^L \bar{p} \frac{\partial A}{\partial z} \bar{v} \, dz + \int_0^L \oint_{C_z} \boldsymbol{\sigma}_D(\bar{u}) \cdot (\mathbf{e}_z \otimes \mathbf{n}_w) \bar{v} \, dl \, dz - \int_0^L f^z \bar{v} \, dz \\
& + \int_{\Omega_2} \rho \frac{\partial \mathbf{u}_2}{\partial t} \Big|_{\mathbf{Y}} \cdot \mathbf{v}_2 \, d\mathbf{x} + \int_{\Omega_2} \rho \nabla \mathbf{u}_2(\mathbf{u}_2 - \mathbf{w}) \cdot \mathbf{v}_2 \, d\mathbf{x} \\
& - \int_{\Omega_2} p_2 \operatorname{div} \mathbf{v}_2 \, d\mathbf{x} + \int_{\Omega_2} \boldsymbol{\sigma}_D(\mathbf{u}_2) \cdot \boldsymbol{\varepsilon}(\mathbf{v}_2) \, d\mathbf{x} - \int_{\Omega_2} \mathbf{f} \cdot \mathbf{v}_2 \, d\mathbf{x} - \int_{\Gamma_{w_2}} \mathbf{t}_w \cdot \mathbf{v}_2 \, d\Gamma \\
& + \int_{\Gamma_c} [\gamma \bar{r}_1(\mathbf{v}_2 \cdot \mathbf{n}_1 - \bar{v}) + (1 - \gamma) \mathbf{r}_2 \cdot (\mathbf{v}_2 - \bar{v} \mathbf{n}_1)] \, d\Gamma \\
& + \int_{\Gamma_c} [\gamma \bar{s}_1(\mathbf{u}_2 \cdot \mathbf{n}_1 - \bar{u}) + (1 - \gamma) \mathbf{s}_2 \cdot (\mathbf{u}_2 - \bar{u} \mathbf{n}_1)] \, d\Gamma = 0 \\
& \forall (\mathbf{v}, \mathbf{s}_1, \mathbf{s}_2) \in \mathcal{V}_d \times \mathcal{Z}_1 \times \mathcal{Z}_2. \quad (29)
\end{aligned}$$

Concerning the mass conservation, from equation (23) we have

$$\begin{aligned}
& \frac{d}{dt} \int_{\Omega_1} \rho q_1 \, d\mathbf{x} - \int_{\Omega_1} \rho(\mathbf{u}_1 - \mathbf{w}) \cdot \nabla q_1 \, d\mathbf{x} + \int_{\Gamma_1} \rho(\mathbf{u}_1 - \mathbf{w}) \cdot \mathbf{n}_1 q_1 \, d\Gamma + \\
& \frac{d}{dt} \int_{\Omega_2} \rho q_2 \, d\mathbf{x} - \int_{\Omega_2} \rho(\mathbf{u}_2 - \mathbf{w}) \cdot \nabla q_2 \, d\mathbf{x} + \int_{\Gamma_2} \rho(\mathbf{u}_2 - \mathbf{w}) \cdot \mathbf{n}_2 q_2 \, d\Gamma \\
& = 0 \quad \forall q \in \mathcal{Q}_d, \quad (30)
\end{aligned}$$

where  $q = (q_1, q_2) \in \mathcal{Q}_d = \mathcal{Q}_1 \times \mathcal{Q}_2$ . From this expression it can be easily verified, by introducing assumptions (26), that

$$\int_0^L \rho \frac{\partial A}{\partial t} \bar{q} \, dz + \int_0^L \rho \frac{\partial(A\bar{u})}{\partial z} \bar{q} \, dz + \int_{\Omega_2} \rho \operatorname{div} \mathbf{u}_2 q_2 \, d\mathbf{x} = 0 \quad \forall q \in \mathcal{Q}_d. \quad (31)$$

## 4.2 Euler equations

Let us obtain the Euler equations related to variational expression (29) and (31). Recall that over  $\Gamma_{\text{in}}$  and  $\Gamma_{\text{out}}$  we impose a Dirichlet boundary condition.

Thus, in the sense of distributions it is possible to write from (29) the following

$$\begin{aligned}
& \int_0^L \left[ \rho A \frac{\partial \bar{u}}{\partial t} + \rho A \bar{u} \frac{\partial \bar{u}}{\partial z} + \frac{\partial(A\bar{p})}{\partial z} - \frac{\partial}{\partial z} \left( \bar{\boldsymbol{\sigma}}_D(\bar{u}) \cdot (\mathbf{e}_z \otimes \mathbf{e}_z) \right) - \bar{p} \frac{\partial A}{\partial z} \right. \\
& \quad \left. + \oint_{C_z} \boldsymbol{\sigma}_D(\bar{u}) \cdot (\mathbf{e}_z \otimes \mathbf{n}_w) \, dl - f^z \right] \bar{v} \, dz \\
& + \int_{\Omega_2} \left[ \rho \frac{\partial \mathbf{u}_2}{\partial t} \Big|_{\mathbf{Y}} + \rho \nabla \mathbf{u}_2(\mathbf{u}_2 - \mathbf{w}) + \nabla p_2 - \operatorname{div} \boldsymbol{\sigma}_D(\mathbf{u}_2) - \mathbf{f} \right] \cdot \mathbf{v}_2 \, d\mathbf{x} \\
& \left[ -A_c \bar{p} + A_c \bar{\boldsymbol{\sigma}}_D(\bar{u}) \cdot (\mathbf{e}_z \otimes \mathbf{e}_z) - \left( \gamma A_c \bar{r}_1 + (1 - \gamma) \int_{\Gamma_c} \mathbf{r}_2 \cdot \mathbf{n}_1 \, d\Gamma \right) \right] \bar{v} \Big|_{z=L} \\
& + \int_{\Gamma_c} \left[ (-p_2 \mathbf{I} + \boldsymbol{\sigma}_D(\mathbf{u}_2)) \mathbf{n}_2 + \gamma \bar{r}_1 \mathbf{n}_1 + (1 - \gamma) \mathbf{r}_2 \right] \cdot \mathbf{v}_2 \, d\Gamma \\
& + \int_{\Gamma_{w_2}} \left[ (-p_2 \mathbf{I} + \boldsymbol{\sigma}_D(\mathbf{u}_2)) \mathbf{n}_2 - \mathbf{t}_w \right] \cdot \mathbf{v}_2 \, d\Gamma \\
& + \gamma \bar{s}_1 \left[ -A_c \bar{u} + \int_{\Gamma_c} \mathbf{u}_2 \cdot \mathbf{n}_1 \, d\Gamma \right] + (1 - \gamma) \left[ \int_{\Gamma_c} (\mathbf{u}_2 - \bar{u} \mathbf{n}_1) \cdot \mathbf{s}_2 \, d\Gamma \right] = 0 \\
& \quad \forall (\mathbf{v}, \mathbf{s}_1, \mathbf{s}_2) \in \mathcal{V}_d \times \mathcal{Z}_1 \times \mathcal{Z}_2, \quad (32)
\end{aligned}$$

where  $A_c$  is the value of the area at  $\Gamma_c$ . Also, from (31) we have

$$\int_0^L \rho \left[ \frac{\partial A}{\partial t} + \frac{\partial(A\bar{u})}{\partial z} \right] \bar{q} \, dz + \int_{\Omega_2} \rho \operatorname{div} \mathbf{u}_2 q_2 \, d\mathbf{x} = 0 \quad \forall q \in \mathcal{Q}_d. \quad (33)$$

Hence we recast the following nonlinear system of Euler equations and Weierstrass–Erdmann corner conditions

$$\begin{aligned}
\rho A \frac{\partial \bar{u}}{\partial t} + \rho A \bar{u} \frac{\partial \bar{u}}{\partial z} &= -A \frac{\partial \bar{p}}{\partial z} + \frac{\partial}{\partial z} \left( \bar{\boldsymbol{\sigma}}_D(\bar{u}) \cdot (\mathbf{e}_z \otimes \mathbf{e}_z) \right) \\
&\quad - \oint_{C_z} \boldsymbol{\sigma}_D(\bar{u}) \cdot (\mathbf{e}_z \otimes \mathbf{n}_w) \, dl + f^z \quad \text{in } (0, L) \times (0, T), \quad (34a)
\end{aligned}$$

$$\begin{aligned}
\rho \frac{\partial \mathbf{u}_2}{\partial t} \Big|_{\mathbf{Y}} + \rho \nabla \mathbf{u}_2(\mathbf{u}_2 - \mathbf{w}) &= -\nabla p_2 \\
&\quad + \operatorname{div} \boldsymbol{\sigma}_D(\mathbf{u}_2) + \mathbf{f} \quad \text{in } \Omega_2 \times (0, T), \quad (34b)
\end{aligned}$$

$$\frac{\partial A}{\partial t} + \frac{\partial(A\bar{u})}{\partial z} = 0 \quad \text{in } (0, L) \times (0, T), \quad (34c)$$

$$\operatorname{div} \mathbf{u}_2 = 0 \quad \text{in } \Omega_2 \times (0, T), \quad (34d)$$

$$\mathbf{t}_w = [-p_2 \mathbf{I} + \boldsymbol{\sigma}_D(\mathbf{u}_2)] \mathbf{n}_2 \quad \text{on } \Gamma_{w_2} \times (0, T), \quad (34e)$$

$$\begin{aligned}
\gamma \bar{r}_1 + (1 - \gamma) \frac{1}{A_c} \int_{\Gamma_c} \mathbf{r}_2 \cdot \mathbf{n}_1 \, d\Gamma &= \\
&\quad - \bar{p} + \bar{\boldsymbol{\sigma}}_D(\bar{u}) \cdot (\mathbf{n}_1 \otimes \mathbf{n}_1) \quad \text{in } \{z = L\} \times (0, T), \quad (34f)
\end{aligned}$$

$$\gamma \bar{r}_1 \mathbf{n}_1 + (1 - \gamma) \mathbf{r}_2 = [-p_2 \mathbf{I} + \boldsymbol{\sigma}_D(\mathbf{u}_2)] \mathbf{n}_1 \quad \text{on } \Gamma_c \times (0, T), \quad (34g)$$

$$\gamma \left[ A_c \bar{u} - \int_{\Gamma_c} \mathbf{u}_2 \cdot \mathbf{n}_1 \, d\Gamma \right] = 0 \quad \text{in } \{z = L\} \times (0, T), \quad (34h)$$

$$(1 - \gamma) [\mathbf{u}_2 - \bar{u} \mathbf{n}_1] = 0 \quad \text{on } \Gamma_c \times (0, T), \quad (34i)$$

where point  $z = L$  corresponds to face  $\Gamma_c$  (see Figure 2).

As in the heat transfer problem, when  $\gamma = 1$  we obtain, from equations (34f)–(34g), the following

$$\begin{aligned} \bar{r}_1 &= -\bar{p} + \bar{\boldsymbol{\sigma}}_D(\bar{u}) \cdot (\mathbf{n}_1 \otimes \mathbf{n}_1) && \text{in } \{z = L\} \times (0, T), \\ \bar{r}_1 \mathbf{n}_1 &= [-p_2 \mathbf{I} + \boldsymbol{\sigma}_D(\mathbf{u}_2)] \mathbf{n}_1 && \text{on } \Gamma_c \times (0, T). \end{aligned} \quad (35)$$

Therefore, combining these expressions and from equation (34h) we finally arrive to

$$[-p_2 \mathbf{I} + \boldsymbol{\sigma}_D(\mathbf{u}_2)] \mathbf{n}_1 = [-\bar{p} + \bar{\boldsymbol{\sigma}}_D(\bar{u}) \cdot (\mathbf{n}_1 \otimes \mathbf{n}_1)] \mathbf{n}_1 \quad \text{on } \Gamma_c \times (0, T), \quad (36a)$$

$$A_c \bar{u} = \int_{\Gamma_c} \mathbf{u}_2 \cdot \mathbf{n}_1 \, d\Gamma \quad \text{in } \{z = L\} \times (0, T), \quad (36b)$$

that may be read, again roughly speaking, as a case where the 1D model feeds the 3D model with a constant Neumann boundary condition, whilst the 3D model supplies the 1D model with a Dirichlet boundary condition. Observe that the variational formulation naturally gives the continuity in the quantities of interest, namely flow rate and normal traction.

On the other hand, if  $\gamma = 0$  we arrive, in a similar manner, to the following expressions

$$\begin{aligned} \frac{1}{A_c} \int_{\Gamma_c} [-p_2 + \boldsymbol{\sigma}_D(\mathbf{u}_2) \cdot (\mathbf{n}_1 \otimes \mathbf{n}_1)] \, d\Gamma = \\ -\bar{p} + \bar{\boldsymbol{\sigma}}_D(\bar{u}) \cdot (\mathbf{n}_1 \otimes \mathbf{n}_1) \quad \text{in } \{z = L\} \times (0, T), \end{aligned} \quad (37a)$$

$$\mathbf{u}_2 = \bar{u} \mathbf{n}_1 \quad \text{on } \Gamma_c \times (0, T), \quad (37b)$$

where, contrarily to the previous case, the 1D model provides the 3D model with a constant Dirichlet boundary condition, while the 3D model feeds the 1D model with a Neumann boundary condition. Then, in this case, the variational principle gives the continuity in the velocity field and in the mean normal traction.

Also, it is worth noticing that the governing variational principle stated in this work leads to those formulations mentioned in [10,34], that are aimed at handling problems with defective boundary conditions. Note that in this case we have extended the formulation for a larger class of problems. Indeed, consider  $\gamma = 1$ . On one hand we can assume that  $Q_c$  is known (we are in this case not interested in what happens in domain  $\Omega_1$ ) and then we have

the *prescribed flow rate problem* treated in references [10,34]. In this case  $\bar{r}_1$  represents the associated Lagrange multiplier that enforces the given flow rate. On the other hand, if what we know is  $\bar{r}_1 = -\bar{p}$  (again we are forgetting what occurs in  $\Omega_1$ ) then we recover the so called *mean pressure problem*, and the flow rate  $Q_c$  is a mere consequence.

Fluid over domain  $\Omega_2$  is hereafter considered as Newtonian, that is

$$\boldsymbol{\sigma}_D(\mathbf{u}_2) = 2\mu\boldsymbol{\varepsilon}(\mathbf{u}_2), \quad (38)$$

while for domain  $\Omega_1$  the following constitutive law is considered, given for simplicity in cylindrical coordinates  $(r, \theta, z)$

$$\boldsymbol{\sigma}_D(\bar{u}) = \begin{pmatrix} 0 & 0 & C\bar{u}r \\ 0 & 0 & 0 \\ C\bar{u}r & 0 & 0 \end{pmatrix}, \quad (39)$$

with  $C = -\frac{4\pi\mu}{A}$ .

**Remark 3** *As far as constitutive laws are concerned note that it is possible to establish different constitutive behaviors for both domains  $\Omega_1$  and  $\Omega_2$ , since expressions  $\boldsymbol{\sigma}_D(\bar{u})$  and  $\boldsymbol{\sigma}_D(\mathbf{u}_2)$  need not be in compliance with any compatibility condition between them.*

Therefore, assuming an axisymmetric pipe, the momentum equation (34a) results

$$\rho A \frac{\partial \bar{u}}{\partial t} + \rho A \bar{u} \frac{\partial \bar{u}}{\partial z} = -A \frac{\partial \bar{p}}{\partial z} - 8\pi\mu\bar{u} + f^z \quad \text{in } (0, L) \times (0, T), \quad (40)$$

thus incorporating those classical frictional terms seen in the literature for the 1D model [1,15,24], whilst equation (34f) now is

$$\gamma\bar{r}_1 + (1 - \gamma) \frac{1}{A_c} \int_{\Gamma_c} \mathbf{r}_2 \cdot \mathbf{n}_1 \, d\Gamma = -\bar{p} \quad \text{in } \{z = L\} \times (0, T). \quad (41)$$

For implementation purposes we continue with  $\gamma = 1$  since for this choice we recover the exact solution of a total developed velocity profile in the stationary case.

Certainly, the problem in terms of the Euler equations is the following

$$\rho A \frac{\partial \bar{u}}{\partial t} + \rho A \bar{u} \frac{\partial \bar{u}}{\partial z} = -A \frac{\partial \bar{p}}{\partial z} - 8\pi\mu\bar{u} + f^z \quad \text{in } (0, L) \times (0, T), \quad (42a)$$

$$\rho \frac{\partial \mathbf{u}_2}{\partial t} \Big|_{\mathbf{Y}} + \rho \nabla \mathbf{u}_2 (\mathbf{u}_2 - \mathbf{w}) = -\nabla p_2 + \mu \Delta \mathbf{u}_2 + \mathbf{f} \quad \text{in } \Omega_2 \times (0, T), \quad (42b)$$

$$\frac{\partial A}{\partial t} + \frac{\partial (A\bar{u})}{\partial z} = 0 \quad \text{in } (0, L) \times (0, T), \quad (42c)$$

$$\operatorname{div} \mathbf{u}_2 = 0 \quad \text{in } \Omega_2 \times (0, T), \quad (42d)$$

$$(-p_2 \mathbf{I} + 2\mu \boldsymbol{\varepsilon}(\mathbf{u}_2)) \mathbf{n}_1 = -\bar{p} \mathbf{n}_1 \quad \text{on } \Gamma_c \times (0, T), \quad (42e)$$

$$A_c \bar{u} = \int_{\Gamma_c} \mathbf{u}_2 \cdot \mathbf{n}_1 \, d\Gamma \quad \text{on } \Gamma_c \times (0, T). \quad (42f)$$

Equation (42e) stands for the continuity of the traction vector at  $\Gamma_c$ , while expression (42f) is the counterpart of the mass conservation at  $\Gamma_c$ .

Consequently, the general setting proposed here allowed us to obtain not only the equilibrium equations for both models, but also the corresponding coupling terms that are now naturally derived since they are implied within the governing variational principle.

Notice that when the set of equations (42), or equivalently (29)–(31), is intended to model the fully coupled fluid–structure interaction problem that arises in the context of hemodynamics, it must be complemented with appropriate relations characterizing the structural behavior of the vessel wall, as will be done in Section 5.

## 5 Approximate solutions

This section is devoted to present the approximation techniques in order to find approximate solutions for the problem treated in the previous section. Before introducing such a numerical scheme, it is necessary to specify the arterial wall behavior in order to characterize the derived fluid–structure interaction model. Accordingly, we choose a simple model such that corresponding counterpart expressions at both parts of the domain (3D and 1D parts) can be given in order to recover an analogous behavior at both sides of the coupling interfaces. Hence we will use the *independent ring model* [14,19,20] because of its simplicity and also it leads to realistic results. The corresponding equations

for both 1D and 3D domains are the following

$$\bar{p} = \bar{p}_0 + \frac{E\pi R_0 h_0}{A} \left( \sqrt{\frac{A}{A_0}} - 1 \right) + \frac{k\pi R_0 h_0}{A} \frac{1}{2\sqrt{A_0 A}} \frac{\partial A}{\partial t} \quad \text{in } (0, L) \times (0, T), \quad (43a)$$

$$p_2 = p_{20} + \frac{Eh}{R_0^2} \zeta + \frac{kh}{R_0^2} \frac{\partial \zeta}{\partial t} \quad \text{on } \Gamma_{w_2} \times (0, T), \quad (43b)$$

where index 0 denotes reference values,  $\zeta$  is a scalar representing the wall displacement in the direction of the outward unit normal vector,  $E$  is the effective Young modulus,  $k$  is the fluidity of the wall and  $R$  and  $h$  are the wall radius (in the transversal direction) and wall thickness respectively.

As a consequence of the previous choice, the resultant 1D model becomes predominantly hyperbolic in response. Thus, the canonical form of equations (42a)–(42c) along the characteristics lines is more appropriate for deriving numerical schemes [7,28]. Therefore, it will be used as the starting point in order to obtain an approximate solution in terms of the flow rate  $Q = A\bar{u}$ , the cross sectional area  $A$  and the pressure  $\bar{p}$ . Notice that this transformation only affects terms defined on the interior of the one dimensional domain, and no modifications on the boundary terms are introduced.

Correspondingly, from equation (43b) we compute the displacement  $\zeta$ , from which we obtain the displacement  $\gamma_{\mathbf{Y}}$  of the ALE frame of reference by solving some well posed problem. In this work a Laplace equation is employed in order to extend the wall displacements to the interior of  $\Omega_2$ . Finally, the velocity  $\mathbf{w}$  of the ALE formulation is directly computed taking the time derivatives of the field  $\gamma_{\mathbf{Y}}$ . Therefore, since we know over  $\Gamma_{w_2}$  the velocity field  $\mathbf{w}$  this is the moment in which we could impose easily the no-slip Dirichlet boundary condition by making  $\mathbf{u}_2|_{\Gamma_{w_2}} = \mathbf{w}$  on  $\Gamma_{w_2}$  instead of considering the equivalent Neumann boundary condition avoiding the evaluation of the corresponding traction  $\mathbf{t}_w$ .

With these considerations, rewriting problem given by equations (29) and (31) eliminating the additional unknown  $\bar{r}_1$  since it is known from equation (41), also considering constitutive relations (38) and (39), and in view of equations (43) we obtain the complete formulation written in terms of the actual unknowns for this problem: *for every*  $t \in (0, T)$ , *find*  $(Q, A, \bar{p}, \mathbf{u}_2, p_2, \gamma_{\mathbf{Y}}) \in \mathcal{W}$

such that

$$\begin{aligned}
& \int_0^L \rho \left( \frac{DQ}{Dt} \Big|_{(-)} - f^+ \frac{DA}{Dt} \Big|_{(-)} - \bar{g} \right) \frac{\bar{Q}}{\lambda_1} dz \\
& \quad + \int_0^L \rho \left( \frac{DQ}{Dt} \Big|_{(+)} - f^- \frac{DA}{Dt} \Big|_{(+)} - \bar{g} \right) \frac{\bar{Q}}{\lambda_1} dz \\
& \quad + \int_{\Omega_2} \rho \frac{\partial \mathbf{u}_2}{\partial t} \Big|_{\mathbf{Y}} \cdot \mathbf{v}_2 d\mathbf{x} + \int_{\Omega_2} \rho \nabla \mathbf{u}_2 (\mathbf{u}_2 - \mathbf{w}) \cdot \mathbf{v}_2 d\mathbf{x} \\
& - \int_{\Omega_2} p_2 \operatorname{div} \mathbf{v}_2 d\mathbf{x} + 2 \int_{\Omega_2} \mu \boldsymbol{\varepsilon}(\mathbf{u}_2) \cdot \boldsymbol{\varepsilon}(\mathbf{v}_2) d\mathbf{x} - \int_{\Omega_2} \mathbf{f} \cdot \mathbf{v}_2 d\mathbf{x} - \boxed{\int_{\Gamma_c} \bar{p} \mathbf{n}_1 \cdot \mathbf{v}_2 d\Gamma} \\
& + \boxed{\int_{\Gamma_c} \rho (\mathbf{u}_2 \cdot \mathbf{n}_1 - \bar{u}) \frac{\bar{Q}}{\lambda_3} d\Gamma} = 0 \quad \forall (\bar{Q}, \mathbf{v}_2) \in \mathcal{W}_{\delta Q} \times W_{\delta \mathbf{u}_2}, \quad (44a)
\end{aligned}$$

$$\begin{aligned}
& \int_0^L \rho f^+ \left( \frac{DQ}{Dt} \Big|_{(-)} - f^+ \frac{DA}{Dt} \Big|_{(-)} - \bar{g} \right) \frac{\bar{A}}{\lambda_2} dz \\
& \quad + \int_0^L \rho f^- \left( \frac{DQ}{Dt} \Big|_{(+)} - f^- \frac{DA}{Dt} \Big|_{(+)} - \bar{g} \right) \frac{\bar{A}}{\lambda_2} dz + \int_{\Omega_2} \rho \operatorname{div} \mathbf{u}_2 q_2 d\mathbf{x} \\
& = 0 \quad \forall (\bar{A}, q) \in \mathcal{W}_{\delta A} \times \mathcal{W}_{\delta p_2}, \quad (44b)
\end{aligned}$$

$$\int_{\Omega_2} \boldsymbol{\kappa} \nabla \boldsymbol{\gamma}_{\mathbf{Y}} \cdot \nabla \mathbf{v}_{\mathbf{Y}} d\mathbf{x} = 0 \quad \forall \mathbf{v}_{\mathbf{Y}} \in \mathcal{W}_{\delta \boldsymbol{\gamma}_{\mathbf{Y}}}, \quad (44c)$$

$$\bar{p} = \bar{p}_0 + \frac{E\pi R_0 h_0}{A} \left( \sqrt{\frac{A}{A_0}} - 1 \right) + \frac{k\pi R_0 h_0}{A} \frac{1}{2\sqrt{A_0 A}} \frac{\partial A}{\partial t} \quad \text{in } (0, L), \quad (44d)$$

$$p_2 = p_{20} + \frac{ER}{R_0^2} \zeta + \frac{kR}{R_0^2} \frac{\partial \zeta}{\partial t} \quad \text{on } \Gamma_{w_2}, \quad (44e)$$

$$\mathbf{w} = \frac{\partial \boldsymbol{\gamma}_{\mathbf{Y}}}{\partial t} \quad \text{in } \Omega_2. \quad (44f)$$

In expressions (44a) and (44b) quantities  $\frac{D(\cdot)}{Dt} \Big|_{(\pm)}$  denote total time derivatives with respect to the characteristics lines corresponding to celerities  $f^\pm = \frac{Q}{A} \pm c$ , being  $c = \sqrt{\frac{A}{\rho} \frac{\partial \bar{p}}{\partial A}}$  the speed of sound into the vessel, and function  $\bar{g}$  is given by  $\bar{g} = f^z - \frac{8\pi\mu}{A} Q$ . Also  $\lambda_i$ ,  $i = 1, 2, 3$ , are constants such that these equations are dimensionally consistent. In equation (44c),  $\boldsymbol{\kappa}$  is a kind of diffusivity tensor that may be set conveniently. In this work the simplest case is used, being  $\boldsymbol{\kappa}$  the identity tensor. Finally, essential boundary conditions are given in function set  $\mathcal{W}$ .

### 5.1 Time discretization and finite element approximation

In this section we describe the numerical techniques used in approximating formulation (44). Since these techniques are well known, we limit ourselves to mentioning, when necessary, the corresponding references and no further details are given. Thus we can summarize the approximation process as follows:

- The variational formulation is discretized first in time by means of a single step finite difference method corresponding to a classical  $\theta$ -scheme for both 1D and 3D parts.
- For variables  $Q$ ,  $A$ ,  $\bar{p}$  of the 1D model  $\mathbb{P}_1$  finite elements are used, while for variables  $\mathbf{u}_2$ ,  $p_2$  of the 3D model  $\mathbb{P}_1^B - \mathbb{P}_1$  finite elements are considered, where supra index  $B$  indicates the use of bubble functions for the velocity field [2]. Degrees of freedom  $\boldsymbol{\gamma}_{\mathbf{Y}}$  are also approximated with  $\mathbb{P}_1$  finite elements, and finally the velocity of the frame of reference  $\mathbf{w}$  is computed from the displacements  $\boldsymbol{\gamma}_{\mathbf{Y}}$  by a backward Euler difference.
- For both 1D and 3D parts, stabilization terms must be included with the aim of avoiding the well known non-physical oscillating solutions present when using a Galerkin approximation. For the 1D model these terms are incorporated along the characteristics lines and correspond to a Galerkin Least Squares formulation [18,33]. For the 3D model the stabilization terms correspond to the Streamline Upwind Petrov Galerkin technique with a suitable stabilization parameter [17].
- Finally, the nonlinearities of the problem are treated in all cases with Picard iterations.

### 5.2 The monolithic scheme

The complete set of discrete equations is then obtained following the guidelines exposed in the previous section. Here we present the resulting linearized algebraic form with the aim of highlighting how coupling terms appear within the monolithic scheme. Thus the discretized problem reads as follows: *for each time step  $t_{n+1}$ ,  $n = 0, 1, 2, \dots, N$ , until a convergence criterion is achieved per-*

form iterations  $k = 1, 2, \dots$ , solving the following system of linear equations

$$\begin{pmatrix} \mathbf{A}_{QQ}^k & 0 & \mathbf{A}_{Q\bar{p}}^k & \mathbf{A}_{Qu_2}^k & 0 & 0 \\ 0 & \mathbf{A}_{AA}^k & \mathbf{A}_{A\bar{p}}^k & 0 & 0 & 0 \\ \mathbf{A}_{\bar{p}Q}^k & 0 & \mathbf{A}_{\bar{p}\bar{p}}^k & 0 & 0 & 0 \\ 0 & 0 & \mathbf{A}_{u_2\bar{p}}^k & \mathbf{A}_{u_2u_2}^k & \mathbf{A}_{u_2p_2}^k & \mathbf{A}_{u_2\gamma_Y}^k \\ 0 & 0 & 0 & \mathbf{A}_{p_2u_2}^k & 0 & 0 \\ 0 & 0 & 0 & 0 & \mathbf{A}_{\gamma_Y p_2}^k & \mathbf{A}_{\gamma_Y \gamma_Y}^k \end{pmatrix} \begin{pmatrix} \mathbf{U}_Q^{k+1}|_{n+1} \\ \mathbf{U}_A^{k+1}|_{n+1} \\ \mathbf{U}_{\bar{p}}^{k+1}|_{n+1} \\ \mathbf{U}_{u_2}^{k+1}|_{n+1} \\ \mathbf{U}_{p_2}^{k+1}|_{n+1} \\ \mathbf{U}_{\gamma_Y}^{k+1}|_{n+1} \end{pmatrix} = \begin{pmatrix} \mathbf{f}_Q^k \\ \mathbf{f}_A^k \\ \mathbf{f}_{\bar{p}}^k \\ \mathbf{f}_{u_2}^k \\ \mathbf{f}_{p_2}^k \\ \mathbf{f}_{\gamma_Y}^k \end{pmatrix}. \quad (45)$$

Here, at time  $t_{n+1}$  and for unknowns  $X, Y$ ,  $\mathbf{A}_{XY}^k$  denote the corresponding block computed in the iteration  $k$ ,  $\mathbf{U}_X^{k+1}|_{n+1}$  the nodal degrees of freedom in the iteration  $k + 1$  and  $\mathbf{f}_X^k$  the forcing terms in the iteration  $k$ .

In the system of linear equations (45) blocks  $\mathbf{A}_{Qu_2}^k$  and  $\mathbf{A}_{u_2\bar{p}}^k$  represent the algebraic counterpart of the coupling terms between both 1D and 3D models boxed in expressions (44). In particular, these matrixes comprise the coupling relation between the degrees of freedom of the 1D node located at  $z = L$  and the 3D nodes that lie on boundary  $\Gamma_c$ .

The algebraic form (45) was used for computations in all the examples presented in this work, and was solved using a Preconditioned Conjugated Gradient Square method [29]. The result is a robust numerical scheme that efficiently manages the coupling of multidimensional models.

Alternatively, a decoupled numerical scheme may be devised in case of working with validated stand-alone 1D and 3D FEM codes. In this case we can split the computations by performing iterations between the 1D and 3D subproblems. In this situation the staggered counterpart of system (45) would read as follows: *for each time step  $t_{n+1}$ ,  $n = 0, 1, \dots, N$ , until a convergence criterion is achieved perform iterations  $k = 0, 1, \dots$ , solving*

- i.  $\mathbf{A}_{1D}^k \mathbf{U}_{1D}^{k+1}|_{n+1} = \mathbf{f}_{1D}^{k,\omega}$  1D problem,
- ii.  $\mathbf{A}_{3D}^k \mathbf{U}_{3D}^{k+1}|_{n+1} = \mathbf{f}_{3D}^{k,\omega}$  3D problem,

where indexes 1D and 3D correspond to the subblocks of the 1D and 3D problem respectively, in particular we have

$$\mathbf{f}_{1D}^{k,\omega} = \begin{pmatrix} \tilde{\mathbf{f}}_Q^{k,\omega} \\ \mathbf{f}_A^k \\ \mathbf{f}_{\bar{p}}^k \end{pmatrix} \quad \mathbf{f}_{3D}^{k,\omega} = \begin{pmatrix} \tilde{\mathbf{f}}_{u_2}^{k,\omega} \\ \mathbf{f}_{p_2}^k \\ \mathbf{f}_{\gamma_Y}^k \end{pmatrix}, \quad (46)$$

and where

$$\begin{aligned}\tilde{\mathbf{f}}_Q^{k,\omega} &= \mathbf{f}_Q^k - \left[ \omega \mathbf{A}_{Q\mathbf{u}_2}^k \mathbf{U}_{\mathbf{u}_2}^k|_{n+1} + (1 - \omega) \mathbf{A}_{Q\mathbf{u}_2}^k \mathbf{U}_{\mathbf{u}_2}^{k-1}|_{n+1} \right], \\ \tilde{\mathbf{f}}_{\mathbf{u}_2}^{k,\omega} &= \mathbf{f}_{\mathbf{u}_2}^k - \left[ \omega \mathbf{A}_{\mathbf{u}_2\bar{p}}^k \mathbf{U}_{\bar{p}}^{k+1}|_{n+1} + (1 - \omega) \mathbf{A}_{\mathbf{u}_2\bar{p}}^k \mathbf{U}_{\bar{p}}^k|_{n+1} \right],\end{aligned}\tag{47}$$

being  $0 < \omega \leq 1$  a subrelaxation parameter that acts between subdomain iterations. The decoupling scheme presented here corresponds to a Gauss-Seidel decomposition, and the well-posedness of both problems is accounted for by contributions in forcing terms  $\tilde{\mathbf{f}}_Q^{k,\omega}$  and  $\tilde{\mathbf{f}}_{\mathbf{u}_2}^{k,\omega}$ .

## 6 Numerical assessments

In this section several situations are considered. The first example illustrates the case for which we have a fairly short-wavelength wave propagating along a pipe simulated by using 3D and 1D models. Here we encounter a non-physical response of the model due to the appearance of spurious reflections. The next three examples are related to the direct application of the formulation developed to the cardiovascular modelling. In particular, the third one exemplifies all the potentialities of using this kind of model, being a clear situation for which other ways of imposing boundary conditions are rather cumbersome to implement. Other examples in this direction can be found in [4,22].

In all these examples we use 3D geometries embedded in a 1D model for which we have two or even three coupling interfaces. Consequently, we perform comparisons at nodes placed at coupling interfaces for two situations: when solving with just the pure 1D model and when using the 3D-1D formulation proposed in this work.

The nomenclature used in describing the 3D geometry and properties in the examples is the following

$L$  : length of the vessel,                       $R$  : radius of the vessel,  
 $h$  : thickness of the arterial wall,       $E$  : Young modulus of the arterial wall,  
 $k$  : fluidity of the arterial wall,       $C$  : speed of sound into the vessel,  
 $p_0$  : reference pressure.

### 6.1 Case 1: Wave travelling along a dimensionally heterogeneous domain

This first example has the purpose of presenting a simple situation for which we put in evidence the effective coupling between models of different dimensionality. We use the configuration shown in Figure 4, where we have an en-

trance represented by a pipe considered as a 1D model and an exit modelled in the same way, whereas a 3D model is used connecting those regions. We set a pressure boundary condition at the entrance by a curve of the form  $p(t) = p_{\max} \sin^2\left(\frac{\pi t}{t_F}\right)$ , with  $p_{\max} = 10000 \text{ dyn/cm}^2$  and  $t_F = 0.005 \text{ sec}$  for  $0 \leq t \leq t_F$ , and  $p(t) = 0$  for  $t > t_F$ . This curve is also shown in Figure 4. All the geometrical and mechanical properties are equal for both models so as to keep the consistency of the whole model. Being  $L_T$  the total length and  $L_{3D}$  just the corresponding one to the 3D model, it is  $L_T = 25 \text{ cm}$ ,  $L_{3D} = 5 \text{ cm}$ ,  $R = 0.5 \text{ cm}$ ,  $h = 0.05 \text{ cm}$ ,  $E = 20.0 \cdot 10^6 \text{ dyn/cm}^2$ ,  $k$  is null,  $C = 1000 \text{ cm/sec}$ ,  $p_0$  is null,  $\rho = 1.0 \text{ g/cm}^3$  and  $\mu = 0.4 \text{ poise}$ . The Reynolds number reaches values around  $\text{Re} = 12$  in the peak of the wave. The number of nodes and degrees of freedom for this case is about 41100 and 283400 respectively, while the time step used is about  $\Delta t = 2.5 \cdot 10^{-5} \text{ sec}$  within a total run time  $T = 2.5 \cdot 10^{-2} \text{ sec}$ .

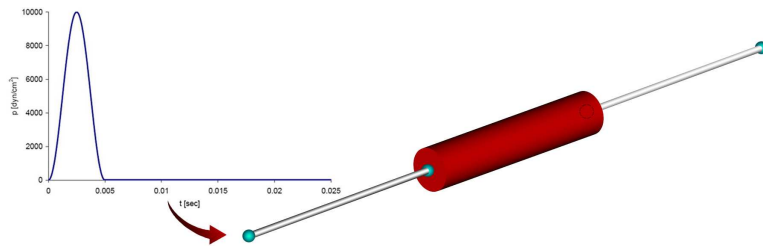


Fig. 4. Cylindrical geometry for case 1 formed by 3D and 1D parts.

In this case we also consider a special situation that emulates the absence of viscosity. For the 1D model this can be done without any problem, while for the 3D model we assume a total slip condition in the axial direction over boundary  $\Gamma_{w2}$ .

The sequence of Figures 5 shows the pressure wave (its mean value inside the 3D region) computed with formulation (44) travelling along the 1D–3D–1D domain. The appearance of spurious reflections travelling in the opposite direction when the wave is passing through both coupling interfaces can be clearly appreciated (see Figures 5(b)–5(d)). The amplitude of the reflected wave is about 2.1% of the amplitude of the inflowing wave. This phenomenon can also be noticed in the examples presented in [9,10] with a reflected wave amplitude of approximately 8%. When using the total slip condition over the wall in the 3D domain we observe, according to Figures 6, almost no spurious reflections, that is, the coupling interface is transparent regarding the waves travelling along the mixed domain. The analysis of the results obtained with these examples indicates that the following dimensionless number  $\frac{1}{\text{Re}} \frac{D}{\lambda}$  where  $\text{Re}$  is the Reynolds number,  $D$  is the diameter of the pipe and  $\lambda$  the wavelength, may be considered as an indicator of the presence of spurious reflections. This issue will be further discussed in Section 6.3. For the examples presented in the following the value of this index ensures the almost absence of spurious reflections.

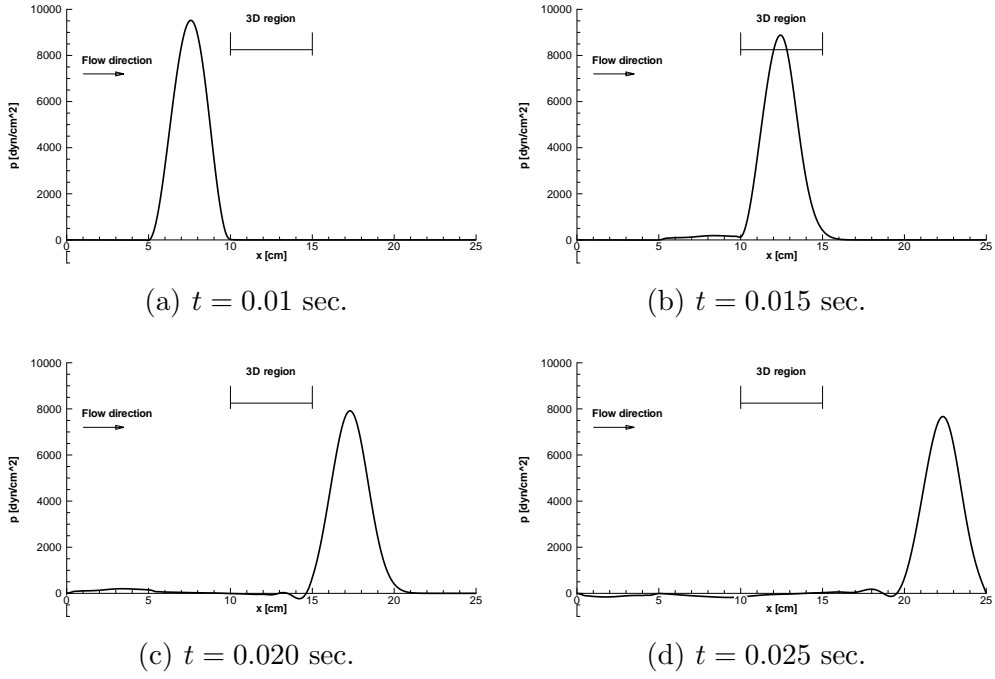


Fig. 5. Results for computations with the derived formulation.

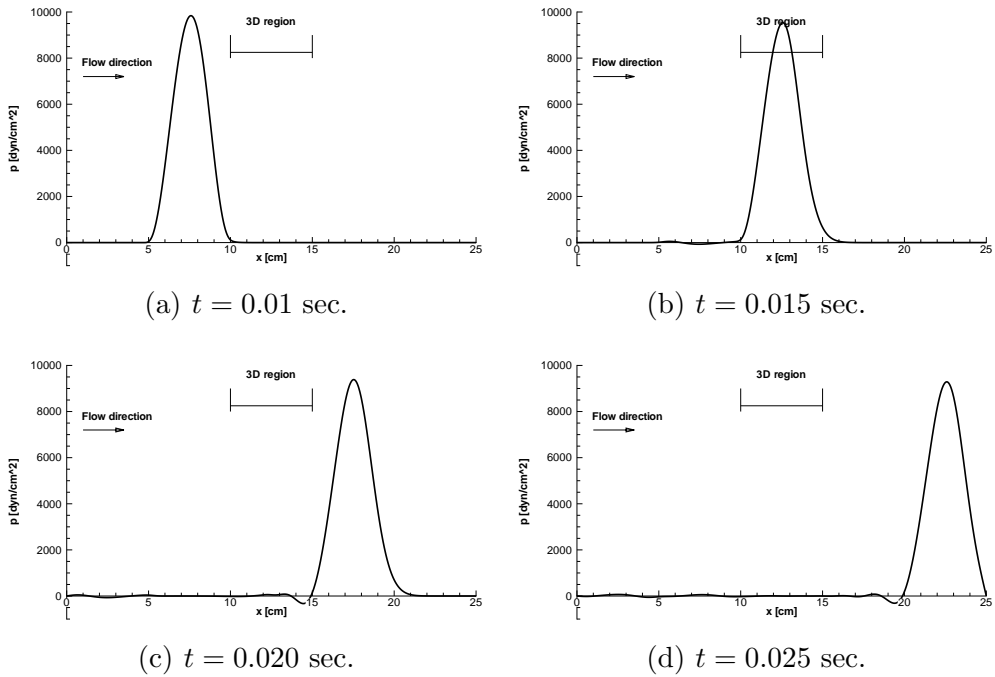


Fig. 6. Results for computations in the simulated absence of viscosity.

## 6.2 Case 2: Applications in cardiovascular modelling

In the applications to hemodynamics the model representing the whole cardiovascular system, with all geometrical and mechanical parameters, was taken

from [3] and is shown in Figure 7(a). The 3D geometries were geometrically and mechanically adapted to the values of the corresponding segments replaced in the 1D arterial tree. The system is fed with two flow rate curves at the aortic root taken from [30,31] and shown in Figure 7(b). Peripheral beds are modelled by Windkessel lumped models.

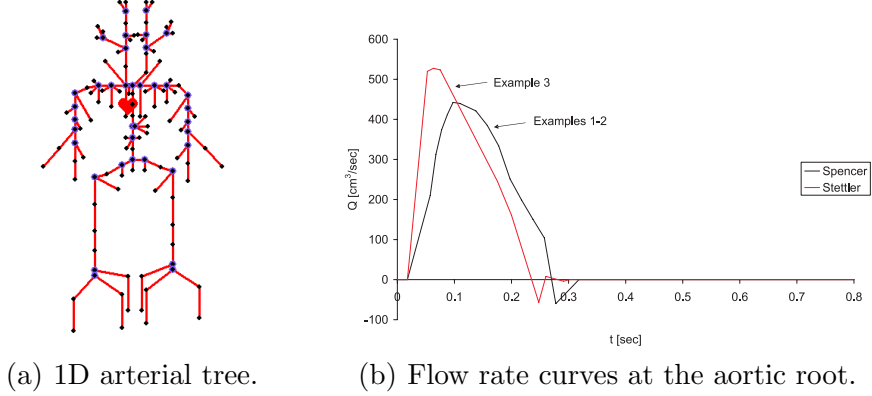


Fig. 7. Arterial tree and the corresponding boundary condition at the aortic root.

It was taken density  $\rho = 1.04 \text{ g/cm}^3$  and viscosity  $\mu = 0.04 \text{ poise}$ , while in all cases the time step used is about  $\Delta t = 1.25 \cdot 10^{-3} \text{ sec}$  within a total run time  $T = 0.8 \text{ sec}$ .

### 6.2.1 Example 1: Blood flow in the abdominal aorta artery

For this example the situation is shown in Figure 8 and the heart ejection curve used is shown in Figure 7(b). We have replaced a segment of the abdominal aorta artery of the 1D arterial tree with a 3D cylindrical geometry. In this example we have  $L = 5.7 \text{ cm}$ ,  $R = 0.57 \text{ cm}$ ,  $h = 0.08 \text{ cm}$ ,  $E = 4.0 \cdot 10^6 \text{ dyn/cm}^2$ ,  $k = 4.44 \cdot 10^4 \text{ dyn sec/cm}^2$ ,  $C = 519.5 \text{ cm/sec}$  and  $p_0 = 1.0 \cdot 10^5 \text{ dyn/cm}^2$ . The Reynolds number reaches values around  $Re = 1700$  in the peak of the systole. The number of nodes and degrees of freedom for this case is about 41300 and 285200 respectively.

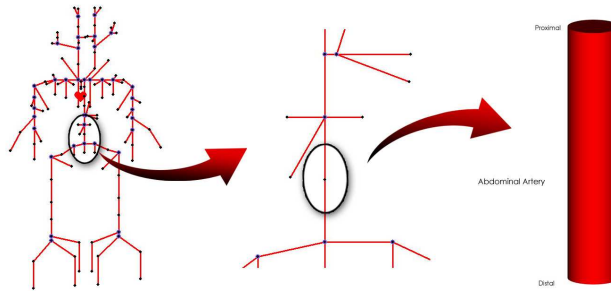


Fig. 8. 3D segment of the abdominal aorta artery embedded in a 1D arterial tree.

Figures 9 show the flow rate  $Q$  and the pressure  $\bar{p}$  at both coupling interfaces named  $\Gamma_p$  and  $\Gamma_d$  indicating proximal and distal locations respectively. In these

figures the results given by formulation (44) together with the pure 1D model are presented. It is observed a good agreement with the results of the pure 1D model, evidencing the suitability of the formulation devised in the present work.

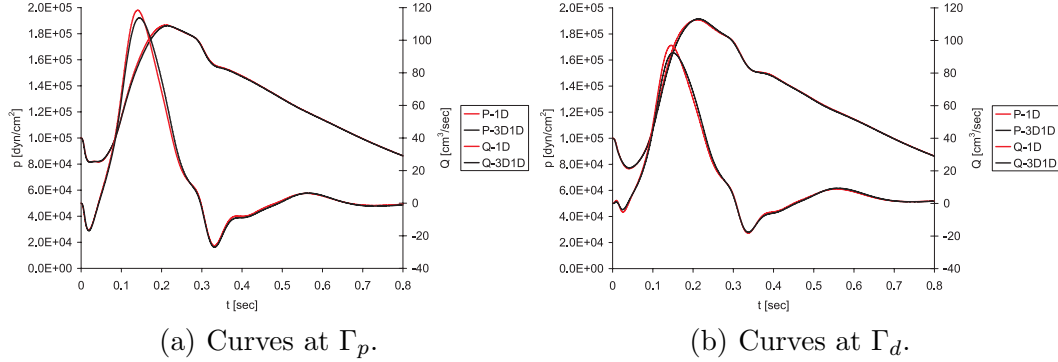


Fig. 9. Flow rate and pressure curves at coupling interfaces  $\Gamma_p$  and  $\Gamma_d$ .

### 6.2.2 Example 2: Blood flow in the external iliac artery

In this situation we have the configuration shown in Figure 10 and the heart ejection curve used is shown in Figure 7(b). We have replaced a segment of the external iliac artery of the 1D arterial tree with a 3D cylindrical geometry. In this example we have  $L = 1.74$  cm,  $R = 0.29$  cm,  $h = 0.055$  cm,  $E = 4.0 \cdot 10^6$  dyn/cm<sup>2</sup>,  $k = 4.44 \cdot 10^4$  dyn sec/cm<sup>2</sup>,  $C = 603.9$  cm/sec and  $p_0 = 1.0 \cdot 10^5$  dyn/cm<sup>2</sup>. The Reynolds number reaches values around  $Re = 885$  in the peak of the systole. The number of nodes and degrees of freedom for this case is about 27800 and 190800 respectively.

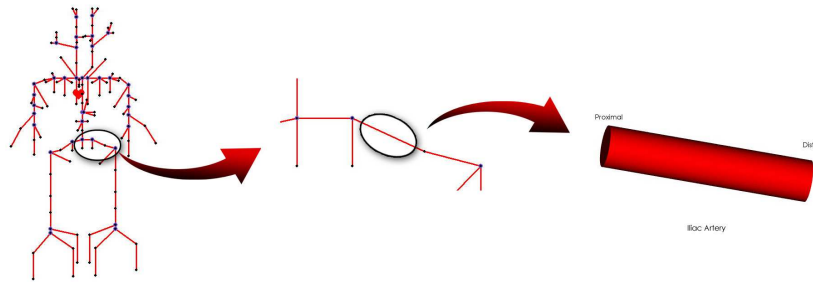


Fig. 10. 3D segment of the external iliac artery embedded in a 1D arterial tree.

Figures 11 show the flow rate  $Q$  and the pressure  $\bar{p}$  at both coupling interfaces  $\Gamma_p$  and  $\Gamma_d$ . Again, in these figures results given by formulation (44) and by the pure 1D model are presented. Once more, there exists a good agreement between the results in terms of the mean quantities.

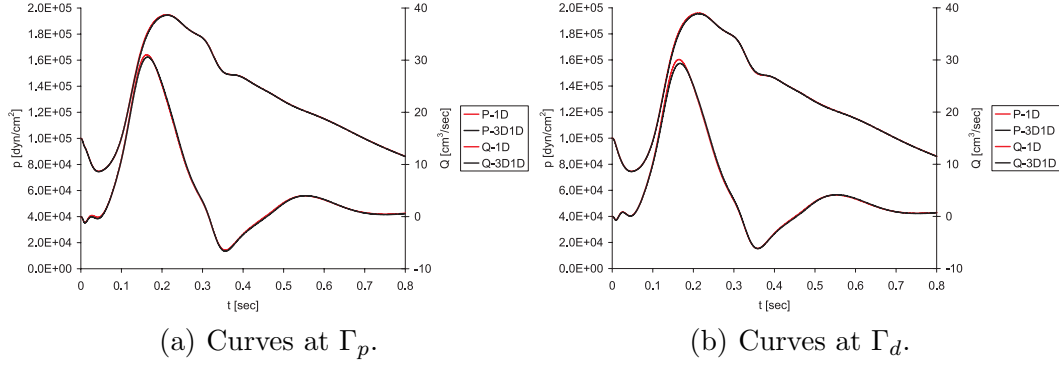


Fig. 11. Flow rate and pressure curves at coupling interfaces  $\Gamma_p$  and  $\Gamma_d$ .

### 6.2.3 Example 3: Blood flow in a stenosed carotid artery bifurcation

In this situation we have the configuration shown in Figure 12 and the heart ejection curve used is also shown in Figure 7(b). We have replaced the district corresponding to the carotid bifurcation of the 1D arterial tree with a 3D standard carotid bifurcation geometry. The goal of this example is to analyze how are perturbed mean quantities (flow rate and pressure) at the coupling interfaces, or even at any location of the 1D model of the arterial tree, when an obstacle such as a simulated stenosis is introduced by strangling the carotid sinus in the 3D district. This kind of analysis can not be performed unless we use this kind of formulations since only here the systemic response of the complete model is properly accounted for. We denote  $N$  the normal situation,  $S80$  a situation with a stenosis of 80% and  $S95$  a situation with a stenosis of 95%. These percentages represent the reduction of the area at the  $SS3$  section (see Figure 13).

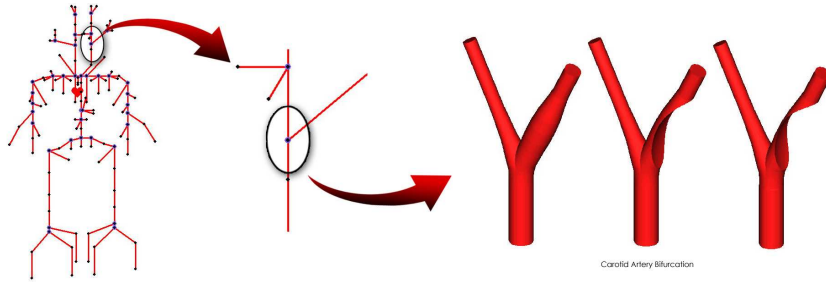
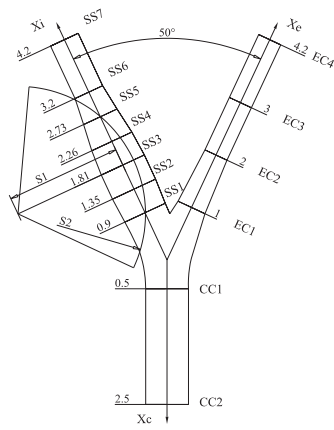


Fig. 12. 3D carotid artery bifurcation embedded in a 1D arterial tree.

Indexes  $c$ ,  $e$  and  $i$  refer to common, external and internal segments. In this example we have  $h = 0.1R$ ,  $E_c = 4.0 \cdot 10^6$  dyn/cm<sup>2</sup>,  $E_e = E_i = 8.0 \cdot 10^6$  dyn/cm<sup>2</sup>,  $k_c = 4.44 \cdot 10^4$  dyn sec/cm<sup>2</sup>,  $k_e = k_i = 8.88 \cdot 10^4$  dyn sec/cm<sup>2</sup> and  $p_0 = 8.0 \cdot 10^4$  dyn/cm<sup>2</sup>. A detailed description of the geometry is given in Figure 13 and in Table 1.

The Reynolds number reaches values around  $Re = 544$  for the  $N$  case,  $Re = 501$  for the  $S80$  case and  $Re = 447$  for the  $S95$  case, always in the peak of the



Section	Diameter [cm]	
CC1	0.74	
CC2	0.74	
SS1	0.77182	
SS2	0.8214	
SS3	0.8214	
SS4	0.76368	
SS5	0.6364	
SS6	0.5254	
SS7	0.5254	
EC1	0.51356	
EC2	0.42032	
EC3	0.42032	
EC4	0.42032	
(stenosis)	80%	95%
S1	2	1.5
S2	2.20535	1.835

Fig. 13. Geometry and stenosis morphology. Table 1. Geometric parameters.

systole and at the entrance of the common carotid. The number of nodes and degrees of freedom for this case is about 69200 and 480500 for the case *S95*, 40400 and 279000 for the case *S80* and 55800 and 386900 for the case *N*.

Figures 14(a), 14(b) and 14(c) show how the mean quantities at coupling interfaces are affected due to the presence of the stenosis. The results correspond to the coupled model. It can be observed that the arterial pulse does not suffer significant perturbations in the case *S80*. Only in the extreme case *S95* appreciable variations of the pressure and flow rate curves are noticeable, especially at the exit of the internal carotid artery. The mean flow supplied through the internal carotid suffers a reduction of 9% with respect to the normal condition. No vasodilation was considered here, although nothing impedes to incorporate this phenomenon in order to improve the simulation.

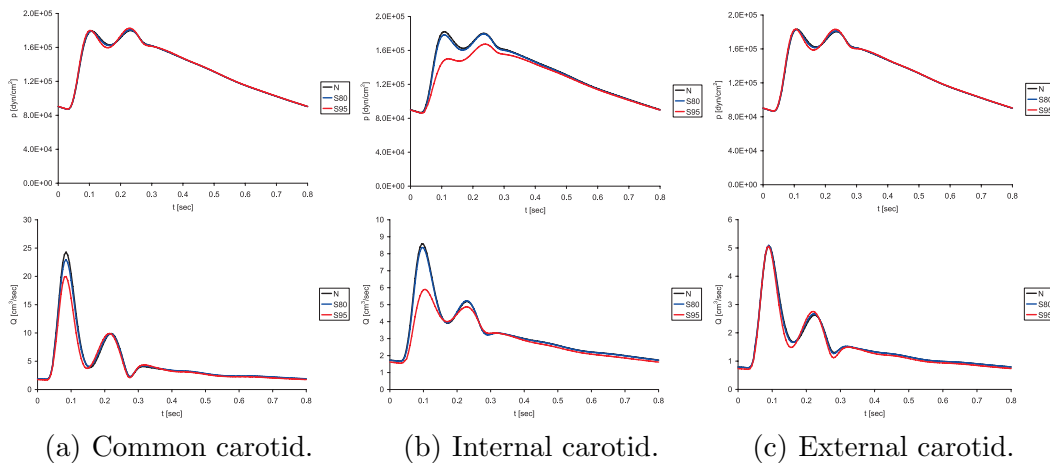


Fig. 14. Comparison of the results for the levels of stenosis considered.

### 6.3 Final remarks

This section is devoted to the discussion of the condition (42e). Certainly, along the derivation of the 1D model some terms associated to viscous effects were neglected. As a result, we obtained the Euler equation at  $\Gamma_c$  given by (42e). Therefore, it is observed that the continuity of pressure is given for two situations: (i) non-viscous flows and (ii) long wavelengths and/or large Reynolds numbers. The second situation was exemplified in Subsection 6.2, whereas the first case was considered in the results shown in the sequence of Figures 6 of the case presented in Subsection 6.1. Here, the absence of viscosity entails the significant reduction of spurious reflections.

As pointed out previously, it is important to characterize when spurious reflections are likely to appear. In this way we perform a dimensionless analysis of the coupling condition related to the normal traction continuity. If we measure the pressure in terms of twice the kinetic energy,  $\rho U^2$ , being  $U$  a representative velocity, and if we take the wavelength  $\lambda$  as a representative length, the dimensionless counterpart of equation (42e) reads as follows

$$-p^* \mathbf{n}_1 = -p_2^* \mathbf{n}_1 + \frac{1}{\text{Re}} \frac{D}{\lambda} \boldsymbol{\varepsilon}^*(\mathbf{u}_2^*) \mathbf{n}_1, \quad (48)$$

where  $D$  is the diameter of the vessel,  $\text{Re} = \frac{\rho U D}{\mu}$  is the Reynolds number and  $(\cdot)^*$  denotes a non-dimensional quantity. Hence, the dimensionless number  $\frac{1}{\text{Re}} \frac{D}{\lambda}$  may be associated to the presence or not of spurious reflections. In examples 1–3, with application in the simulation of the cardiovascular system (see Subsection 6.2), we observe that the smallness of this number allows us to say that we have almost no spurious reflections. This can be seen in the range of values shown in Table 2. In building this table we have used  $\lambda = 5$  cm for the situation of Subsection 6.1 and  $\lambda = 500$  cm for the situation of Subsection 6.2. Consequently, the smallness of the dimensionless number  $\frac{1}{\text{Re}} \frac{D}{\lambda}$  may be used in order to indicate when the model can be considered accurate in the sense of the spurious reflections generated by the coupling interfaces.

	Case 1	Case 2 Example 1	Case 2 Example 2	Case 2 Example 3
$\frac{1}{\text{Re}} \frac{D}{\lambda}$	$4.17 \cdot 10^{-2}$	$1.34 \cdot 10^{-6}$	$1.31 \cdot 10^{-6}$	$2.96 \cdot 10^{-6}$

Table 2

Values of  $\frac{1}{\text{Re}} \frac{D}{\lambda}$  for examples presented in Subsections 6.1 and 6.2.

However, since there exists several other aspects that must be integrated in the analysis of this problem, the previous explanation must be considered as the starting point for further investigation on this matter.

## 7 Conclusions

In this work we have proposed a variational principle that manages possible discontinuities that arise when different underlying kinematics are considered on some partition of a given domain. Consequently, this framework resulted in a suitable and unified strategy that efficiently tackles this kind of problem. For usual situations encountered in cardiovascular modelling we have obtained good results for the simultaneous use of 3D and 1D models, showing the capabilities of the formulation to handle the coupling conditions in a natural way. Moreover, in situations for which classical techniques of imposing boundary conditions could not be applied the model studied here resulted in a versatile tool performing promisingly. From the numerical examples it is possible to see that the spurious reflections are significantly reduced for the non-viscous case. From this we conclude that the role of the viscous shear stress must be a subject of further investigation.

## Acknowledgements

Pablo Javier Blanco (140686/2005–3) was supported by the Brazilian agency CNPq. The support of this agency is gratefully acknowledged.

## References

- [1] M. Anliker, R.L. Rockwell and E. Ogden, Nonlinear analysis of flow pulses and shockwaves in arteries. Part I: derivations and properties of mathematical model, *ZAMP* 22 (1971) 217–246.
- [2] D.N. Arnold, F. Brezzi and M. Fortin, A stable finite element for the Stokes equations, *Calcolo* 21 (1984) 337–344.
- [3] A.P. Avolio, Multi-branched model of the human arterial system, *Med. Biol. Engrg. Comp.* 18 (1980) 709–718.
- [4] P.J. Blanco, I. Larrabide, S.A. Urquiza and R.A. Feijóo, Sensitivity of blood flow patterns to the constitutive law of the fluid, in: *Proc. ECCM2006 - III European Conference on Computational Mechanics Solids, Structures and Coupled Problems in Engineering*, C.A. Mota Soares et al. (Eds.), Lisbon, Portugal, June 2006.
- [5] F. Brezzi and M. Fortin, *Mixed and Hybrid Finite Element Methods*, (Springer-Verlag, New York, 1991).

- [6] C.G. Caro, J.M. Fitz-Gerald, R.C. Schroter, Atheroma and arterial wall shear dependent mass transfer mechanism for atherogenesis, *Proc. Royal Society of London, Biology* B177 (1971) 109–159.
- [7] R. Courant, D. Hilbert, *Methods of Mathematical Physics, Vol. II*, (Interscience Publishers, New York, 1962).
- [8] R.A. Feijóo, L. Bevilacqua, L. Rojas, A variational principle for the Laplace’s operator with applications in the torsion of composite rods, *Int. J. Sol. Struct.* 10 (1974) 1091–1102.
- [9] L. Formaggia, J.F. Gerbeau, F. Nobile and A. Quarteroni, On the coupling of 3D and 1D Navier–Stokes equations for flow problems in compliant vessels, *Comp. Meth. Appl. Mech. Engrg.* 191 (2001) 561–582.
- [10] L. Formaggia, J.F. Gerbeau, F. Nobile and A. Quarteroni, Numerical treatment of defective boundary conditions for the Navier–Stokes equations, *SIAM J. Numer. Anal.* 40 (2002) 376–401.
- [11] D.P. Giddens, C.K. Zarins, S. Glagov, The role of fluid mechanics in the localization and detection of atherosclerosis, *J. Biomech. Engrg.* 115 (1993) 588–594.
- [12] V. Girault and P.-A. Raviart, *Finite Element Methods for Navier–Stokes Equations. Theory and Algorithms*, (Springer–Verlag, Berlin, 1986).
- [13] J.G. Heywood, R. Rannacher and S. Turek, Artificial boundaries and flux and pressure conditions for the incompressible NavierStokes equations, *Int. J. Num. Meth. Fluids* 22 (1996) 325–352.
- [14] R. Holenstein, P. Niederer and M. Anliker, A viscoelastic model for use in predicting arterial pulse waves, *J. Biomech. Engrg.* 102 (1980) 318–325.
- [15] T.J.R. Hughes and J. Lubliner, On the one–dimensional theory of blood flow in the larger vessels, *Math. Biosciences* 18 (1973) 161–170.
- [16] T.J.R. Hughes, W.K. Liu, T.K. Zimmermann, Lagrangian–Eulerian finite element formulation for incompressible viscous flows, *Comp. Meth. Appl. Mech. Engrg.* 29 (1981) 329–349.
- [17] T.J.R. Hughes, L.P. Franca and M. Mallet, A new finite element formulation for computational fluid dynamics: VI. Convergence analysis of the generalized SUPG formulation for linear time–dependent multidimensional advective–diffusive systems, *Comp. Meth. Appl. Mech. Engrg.* 63 (1987) 97–112.
- [18] T.J.R. Hughes, L.P. Franca and G.M. Hulbert, A new finite element formulation for computational fluid dynamics: VIII. The Galerkin/least squares method for advective–diffusive equations, *Comp. Meth. Appl. Mech. Engrg.* 73 (1989) 173–189.
- [19] Y. Kivity and R. Collins, Nonlinear fluid–shell interactions: application to blood flow in large arteries, *Int. Sym. Discrete Meth. Engrg.* (1974) 476–488.

- [20] Y. Kivity and R. Collins, Nonlinear wave propagation in viscoelastic tubes: application to aortic rupture, *J. Biomech.* 7 (1974) 67–76.
- [21] D.N. Ku, D.P. Giddens, C.K. Zarins, S. Glagov, Pulsatile flow and atherosclerosis in the human carotid bifurcation, *Arteriosclerosis* 5 (1985) 293–302.
- [22] I. Larrabide, P.J. Blanco, S.A. Urquiza and R.A. Feijóo, Sensitivity of blood flow in stenosed carotid bifurcation, in: *Proc. ICCB2005 - II International Conference on Computational Bioengineering*, H. Rodrigues et al. (Eds.), Lisbon, Portugal, September 2005.
- [23] R. Löhner, J. Cezbral, O. Soto, P. Yim and J.E. Burgess, Applications of patient-specific CFD in medicine and life sciences, *Int. J. Num. Meth. Fluids* 43 (2003) 637–650.
- [24] P.F. Niederer, Damping mechanisms and shock-like transitions in human arterial tree, *ZAMP* 36 (1985) 204–220.
- [25] M. Oshima, R. Torii, T. Kobayashi, N. Taniguchi and K. Takagi, Finite element simulation of blood flow in the cerebral artery, *Comp. Meth. Appl. Mech. Engrg.* 191 (2001) 661–671.
- [26] K. Perktold and G. Rappitsch, Computer simulation of local blood flow and vessel mechanics in a compliant carotid artery bifurcation model, *J. Biomech.* 28 (1995) 845–856.
- [27] A. Quarteroni, M. Tuveri and A. Veneziani, Computational vascular fluid dynamics: problems, models and methods, *Comp. Vis. Science* 2 (2000) 163–197.
- [28] R.D. Richtmyer and K.W. Morton, *Difference Methods for Initial-Value Problems*, (Interscience Publishers, New York, 1967).
- [29] Y. Saad, SPARSEKIT: a basic tool kit for sparse matrix computation version 2, <http://www.users.cs.umn.edu/~saad/software/SPARSEKIT/sparsekit.html>, University of Illinois (1985).
- [30] M.P. Spencer and A.B. Deninson, The square-wave electro-magnetic flowmeter. Theory of operation and design of magnetic probes for clinical and experimental applications, *I.R.E. Trans. Med. Elect.* 6 (1959) 220–228.
- [31] J.C. Stettler, P. Niederer and M. Anliker, Theoretical analysis of arterial hemodynamics including the influence of bifurcations part I, *Ann. Biomed. Engrg.* 9 (1981) 145-164.
- [32] C.A. Taylor, T.J.R. Hughes and C.K. Zarins, Finite element modeling of three-dimensional pulsatile flow in the abdominal aorta: relevance to atherosclerosis, *Ann. Biomed. Engrg.* 26 (1998) 1–14.
- [33] S.A. Urquiza, P.J. Blanco, M.J. Vénere and R.A. Feijóo, Multidimensional modelling for the carotid artery blood flow, *Comp. Meth. Appl. Mech. Engrg.* 195 (2006) 4002–4017.

- [34] A. Veneziani, C. Vergara, Flow rate defective boundary conditions in haemodynamics simulations, *Int. J. Num. Meth. Fluids* 47 (2005) 803–816.
- [35] I.E. Vignon–Clementel, C.A. Figueroa, K.E. Jansen and C.A. Taylor, Outflow boundary conditions for three–dimensional finite element modeling of blood flow and pressure in arteries, *Comp. Meth. Appl. Mech. Engrg.* 195 (2006) 3776–3796.